PBN-PVT projection modulates negative emotions in mice

Ya-Bing Zhu[1], Rui Zhang[1], Yan Wang[1], Peng-Fei Liu[1], Jin-Bao Li[1], Di Mu[1,*]

[1]Department of Anesthesiology, Shanghai General Hospital, Shanghai Jiao Tong University School of Medicine, Shanghai, China, 201620, China

Correspondence to:

Di Mu, Ph.D.

Email: damonmu@163.com or 018501md@shgh.cn

Department of Anesthesiology, Shanghai General Hospital,

Shanghai Jiao Tong University School of Medicine

No. 650 Xin Song Jiang Road

Shanghai 201620, China.

Abstract

Negative emotions can be described as feelings that cause us to be miserable and sad. Long-lasting negative emotions dampen enthusiasm for life; thus, dealing with negative emotions is essential for individual survival. The parabrachial nucleus (PBN) and the thalamic paraventricular nucleus (PVT) are critical for modulating affections in mice. However, the functional role of the projection from the PBN to the PVT in affection modulation remains elusive. Here, we show that the PBN neurons send dense projection fibers to the PVT and form direct excitatory synapses with the PVT neurons. Activation of the PBN-PVT projections or PVT-projecting PBN neurons induces robust anxiety-like and fear-like behaviors without affecting depression-like and nociceptive behaviors. Inhibition of the PVT-projecting PBN neurons relieves fear-like and aversion-like behaviors. Furthermore, the PVT neurons innervated by the PBN were activated in negative experiences, and activation of these neurons induced anxiety-like behavior. Thus, our study indicates that the PBN-PVT projection modulates negative emotions in mice.

Keywords: Parabrachial nucleus (PBN); thalamic paraventricular nucleus (PVT); negative emotions; fear; anxiety.

Introduction

Threat and injury often induce defensive reactions, such as flight, freezing, hiding *(Öhman and Mineka, 2001)*, and negative emotions, such as fear and anxiety *(Jimenez et al., 2018)*. Such behavioral adaptations and psychological responses are essential for survival, and understanding the mechanisms is of fundamental interest. It's worth noting that the parabrachial nucleus (PBN) in the brainstem plays a critical role in encoding danger signals and promoting affective behavior states to limit harm in response to potential threats *(Campos et al., 2018)*.

The PBN receives the majority of the ascending inputs from the spinal cord

(Todd, 2010) and the PBN neurons respond robustly to nociception, food neophobia, hypercapnia, and threat to maintain homeostasis under stressful or threatening circumstances *(Campos et al., 2018; Kaur et al., 2013)*. The PBN relays this information (visceral malaise, taste, temperature, pain, itch) to brain areas, such as the hypothalamus, the central of the amygdala (CeA), thalamus, insular cortex (IC), and periaqueductal gray (PAG) to participate in diverse physiology process *(Chiang et al., 2019; Palmiter, 2018; Saper, 2016)*. A recent study has found that the subpopulations of PBN have distinct projection patterns and functions *(Chiang et al., 2020)*. The dorsal division PBN (dPBN) neurons projecting to the ventromedial hypothalamus (VMH) and PAG mediate escaping behaviors. In contrast, the external lateral division PBN (elPBN) neurons projecting to the bed nucleus of the stria terminalis (BNST) and the CeA mediate aversion and avoidance memory *(Chiang et al., 2020)*. Optogenetics manipulation of specific outputs from PBN generates a specific function *(Bowen et al., 2020)*. In the thalamus, the intralaminar thalamus nucleus (ILN) is the downstream target of PBN neurons which receive spinal cord inputs and participates in nociception processing *(Deng et al., 2020)*. Besides the ILN nucleus, the thalamic paraventricular nucleus (PVT) is another primary target of the PBN nucleus in the thalamus *(Chiang et al., 2020)*.

The PVT nucleus locates in the dorsal part of the midline thalamus *(Vertes et al., 2015)* and has been heavily implicated in a range of affective behaviors *(Hsu et al., 2014)*. The functional roles of the PVT include diverse processes such as associative learning, arousal, drug addiction, stress, and retrieval of fear memory *(Beas et al., 2018; Do-Monte et al., 2015; Penzo et al., 2015; Ren et al., 2018; Zhu et al., 2018; Zhu et al., 2016)*. The PVT receives a significant amount of inputs from the brainstem (locus coeruleus, PBN, PAG), hypothalamus, prefrontal cortical areas and projects to the infralimbic cortex, nucleus accumbens (NAc), BNST, and CeA *(Kirouac, 2015)*. The convergent signals included the arousal from the hypothalamus *(Ren et al., 2018)*, the

emotional saliency from the prefrontal cortex *(Yamamuro et al., 2020)*, and the stress responsivity from locus coeruleus (LC) *(Beas et al., 2018)* might help to promote the appropriate behavioral responses to environmental challenges. However, despite the substantial improvements in our understanding of the PVT nucleus's neurocircuitry, the direct functional role of the PBN-PVT projection remains mostly unknown.

In this study, we used virus tracing and electrophysiology to dissect the anatomical and functional connection between the PBN nucleus and the PVT nucleus. By using optogenetics and pharmacogenetics approaches, we then demonstrated that the PBN-PVT projection modulates negative emotions in mice.

Results

Functional connectivity pattern of the PBN-PVT projection

The PBN nucleus sends projections to multiple brain areas, including the central nucleus of the amygdala (CeA), thalamus, insular cortex (IC), periaqueductal gray (PAG) *(Chiang et al., 2019)*. Some studies have reported that the PVT could receive input from the PBN nucleus *(Chiang et al., 2020; Li and Kirouac, 2012)*. The detailed morphology of the PBN-PVT projection and whether these two nuclei form direct functional synapses remain unknown.

We used virus tracing and electrophysiological approaches to answer these questions. Most PBN neurons express the vesicular glutamate transporter type 2 (VgluT2) *(Mu et al., 2017)*. Therefore, we used the *VgluT2-ires-Cre* mice combined with the AAV2/8-EF1a-DIO-EGFP virus to specifically label the glutamatergic neurons of the PBN nucleus (*Figure 1A*). Robust expression of AAV2/8-EF1a-DIO-EGFP was found in both the lateral and medial PBN nuclei (*Figure 1B−D*). The $EGFP^+$ fibers were observed from anterior to posterior in the PVT and most of the fibers were located near the midline (*Figure 1E−H*).

Next, we employed the whole-cell patch-clamp recording to examine the

synaptic connectivity between the PBN and the PVT. The PBN neurons were recorded in acute slices prepared from the mice injected with AAV2/8-hSyn-ChR2-mCherry in the left PBN (*Figure 1I−J*). Precisely time-locked action potentials were induced by a train of brief laser pulses (5 Hz, 10 Hz, and 20 Hz) in the current-clamp (*Figure 1K*). We found that optogenetics activation of the PBN projection fibers evoked excitatory postsynaptic currents (EPSCs) in the majority of recorded neurons in PVT (34/52 neurons). The medial PVT showed higher connectivity (bregma -0.94 to -1.82 mm, 27 of 37 cells, 72.97%) than anterior PVT (bregma -0.22 to -0.94 mm, 2 of 6 cells, 33.33%) or posterior PVT (bregma -1.82 to -2.3 mm, 5 of 9 cells, 55.56%, *Figure 1L−N*). The average amplitude of the light-evoked EPSCs was 103.4 ± 11.93 pA (*Figure 1O*). Moreover, the average latency of EPSCs was 3.13 ± 0.29 ms with a jitter of 0.16 ± 0.02 ms (*Figure 1P−Q*), indicating monosynaptic connections between the PBN and the PVT nuclei. The EPSC was sensitive to the Na^+ channel blocker tetrodotoxin (TTX, 1 μM) and was rescued by the K^+ channel blocker 4-aminopyridine (4-AP, 100 μM). The EPSC was further blocked by the AMPA receptor antagonist NBQX (10 μM), confirming the monosynaptic glutamatergic innervation of the PVT neurons by the PBN neurons (*Figure 1R−S*).

To systematically label the PBN neurons that project to the PVT, we injected the retroAAV2/2-hSyn-Cre virus into the PVT nucleus on *Rosa26-tdTomato* mice which could retrogradely label the projection neurons (*Figure 1T−U*). We found that $tdTomato^+$ neurons were bilaterally located in the central subnuclei of lateral PBN (LPBN, 55 ± 5.82 neurons, n = 4 mice) and rarely in the medial PBN (MPBN, 7.75 ± 1.03 neurons, *Figure 1V−W*). These results indicate that bilateral central subnuclei of LPBN project to the medial PVT.

We also observed the PVT nucleus received projections from numerous other regions in the brain, including the prefrontal cortex, the insular cortex, and the suprachiasmatic nucleus (*Figure1−figure supplement 1A−J*), which

were consistent with previous tracing studies *(Kirouac, 2015)*.

Optogenetics activation of PBN-PVT projection induces anxiety-like behaviors and aversion

We injected AAV2/9-EF1a-DIO-ChR2-mCherry virus or AAV2/9-EF1a-DIO-mCherry virus into the bilateral PBN of *VgluT2-ires-Cre* mice and implanted optic fibers above the PVT to activate the PBN-PVT projection selectively (*Figure 2A*). Four weeks after surgery, we found robust expression of ChR2-mCherry (*Figure 2B−C, Figure2−figure supplement 1A−B*) or mCherry (*Figure2−figure supplement 1E−F*) in bilateral PBN neurons and the axon terminals in the PVT (*Figure 2D, Figure2−figure supplement 1C−D, Figure2−figure supplement 1G−H*).

We performed a 15 minutes optogenetics manipulation open field test (OFT, 0−5 minutes laser OFF, 5−10 minutes 20 Hz 473 nm laser ON, 10−15 minutes laser OFF, *Figure 2E*). Optogenetics activation of the efferents from the PBN to the PVT elicited instant running behavior along the chamber wall with a significantly increased velocity in the ChR2 injected mice (*Figure 2F−G*). The ChR2 injected mice rarely entered into the center area of the chamber, represented as a decrease in center time than that of the control group (*Figure 2I*). It's worth noting that the velocity returned to normal once the laser was off, but the time spent in the center was still lower than the control group in the 5 minutes after stimulation (*Figure 2H−I*). These results indicated the change of velocity induced by the optogenetics activation was transient, but the anxiety remained. Although the speed increased during laser ON, the unmoving time of the ChR2 mice during the laser ON period was increased (*Figure2−figure supplement 2A*). Therefore, the laser ON distance and the total distance in 15 minutes were not changed (*Figure2−figure supplement 2B*).

We further divided the laser ON period (5−10 minutes) into the first one minute (5−6 minute) and the last four minutes (6−10 minutes, *Figure2−figure supplement 2C−D*). We found the velocity of the ChR2 mice was increased in

both periods (*Figure 2E*). The unmoving time of ChR2 mice was not changed in 5-6 minute but was significantly increased in the 6−10 minutes (*Figure2−figure supplement 2F*). Consistently, the distance of the ChR2 mice was increased only in the 5−6 minute, but not in 6−10 minutes (*Figure2−figure supplement 2G*). The time spent in the center zone of the ChR2 mice had a decreased tendency in the first 5-6 minute and was significantly decreased in the 6−10 minutes. (*Figure2−figure supplement 2H*). This detailed analysis indicates that optogenetics activation induces a brief but robust running behavior, followed by anxiety-like behaviors, such as unmoving and less time spent in the center.

Besides anxiety, another critical component of negative emotions is aversion. Therefore, we used the real-time placed aversion test (RTPA) to explore the function of optogenetics activation of the PBN-PVT projections (*Figure 2J*). We found that the ChR2 expressing mice spent less time on the side of the chamber in which they received 20 Hz 473 nm laser stimulation, and the aversion was disappeared when the laser was off (*Figure 2K−M*). These results indicate that activation of the PBN-PVT projection is sufficient to induce aversion but could not enable associative aversion conditioning. To further confirm this instant aversion phenomenon, we subjected mice to the cue-dependent optogenetics conditioning test (*Figure 2N*). A 30 seconds auditory conditioning stimulus (CS) co-terminated with 30 seconds of synchronous optogenetics activation of the PBN-PVT projection (US) in this test. The ChR2 expressing mice generated significant freezing behavior after 6 CS-US pairings (*Figure 2O*). However, the freezing behavior to the same context or the CS in a novel context was disappeared on the second day (*Figure 2P−Q*). These results demonstrate that optogenetics activation of the PBN-PVT projection induces instant aversion and freezing but not drives associative fear learning.

Pharmacogenetics activation of the PVT-projecting PBN neurons

induces anxiety-like behaviors and freezing behaviors

We also used pharmacogenetics manipulation and retrograde tracing to confirm the effects of activating the PVT-projecting PBN neurons. We first injected the retoAAV2/2-hSyn-Cre virus into the PVT and AAV2/8-EF1a-DIO-EGFP virus into the PBN (*Figure3−figure supplement 1A*). After four weeks, we found retrogradely labeled LPBN neurons and projection fibers in the PVT (*Figure3−figure supplement 1B−C*). Interestingly, we found nearly no efferent from the PVT-projecting PBN neurons appeared in the CeA (*Figure3−figure supplement 1D*), indicating the PVT-projecting PBN neurons do not send significant collateral projections to the CeA. We further injected the retroAAV2/2-hSyn-Cre virus into the PVT, and the AAV2/9-hSyn-DIO-hM3Dq-mCherry virus or control virus into bilateral PBN nuclei to specifically transduce the PVT-projecting PBN neurons with a designer receptor exclusively activated by designer drugs (DREADDs, *Figure 3A*) *(Armbruster et al., 2007)*. The PVT-projecting PBN neurons could be activated by intraperitoneal injection of clozapine N-oxide dihydrochloride (CNO, *Figure 3B−D*). The region of the virus expression in the PBN nucleus is shown in *Figure3−figure supplement 2A−F*. Consistent with the optogenetics activation results, the hM3Dq group mice spent less time in the center, had more unmoving time, and traveled fewer distances than the mCherry group mice in the OFT (*Figure 3E−I*). At the same time, the velocities were not significantly different (*Figure 3J*). We also found that activation of the PVT-projecting PBN neurons did not affect motor ability in the rotarod test (*Figure3−figure supplement 3G*), which indicates the increased unmoving time is not related to motor deficiency. Besides, the hM3Dq mice showed decreased exploration time of open quadrants in the EZM (*Figure 3K−L*), further indicating that activation of the PBN-PVT pathway could induce anxiety.

Both the running behaviors in optogenetics activation and increased unmoving time in both manipulations indicated that the PBN-PVT projection was also closely linked to fear-like behaviors. Therefore, we further evaluated

freezing behaviors in the fear conditioning chamber and found the hM3Dq mice displayed more freezing behaviors after injection of CNO than control mice (*Figure 3M−N*).

Although activation of the PBN-PVT pathway induced significant anxiety-like behavior, it did not affect the depressive-like behaviors evaluated by the tail suspension test (TST, *Figure3−figure supplement 3A*) and the forced swimming test (FST, *Figure3−figure supplement 3B*). Previous studies have revealed that the PBN receives direct projections from the spinal cord and plays a vital role in pain processing *(Deng et al., 2020; Sun et al., 2020)*. We then assessed whether pharmacogenetic activation of the PVT-projecting PBN neurons affects the nociceptive behaviors. By performing the Von Frey test and Hargreaves test, we found that the basal nociceptive thresholds of mechanical allodynia and thermal hyperalgesia were not affected after pharmacogenetic activation of the PVT-projecting PBN neurons (*Figure3−figure supplement 3C−D*). Given that the distinct mechanism between the reflexive and coping responses induced by nociceptive stimulation *(Huang et al., 2019)*, we also injected formalin into the paw to induce inflammatory pain. Activation of the PVT-projecting PBN neurons did not affect the formalin-evoked licking behaviors (*Figure3−figure supplement 3E−F*). These results indicate that the PBN-PVT projection might not participate in the pain processing.

Inhibition of the PBN-PVT projection rescues the 2-MT-induced and shock-induced fear behaviors

The activation manipulation results prompted us to further investigate whether inhibition of the PBN-PVT projection could relieve the negative emotions. Therefore, the retroAAV2/2-hSyn-Cre virus was injected into the PVT, and the AAV2/9-EF1a-DIO-NpHR3.0-EYFP virus or the AAV2/8-EF1a-DIO-EGFP virus was injected bilaterally into the PBN. The optic fibers were implanted above the PBN to inhibit the PVT-projection PBN neurons specifically (*Figure 4A−C*).

By performing the OFT, we found that direct optogenetics inhibition of the PVT-projecting PBN neurons did not affect the basal emotional states and the locomotion (*Figure4−figure supplement 1A−D*). We used 2-methyl-2-thiazoline (2-MT), a widely used odorant molecule that could generate innate-fear freezing responses in rodents to induce fear-like freezing behaviors *(Isosaka et al., 2015)*. We found that constant 589 nm laser-induced inhibition of the PVT-projecting PBN neurons rescued the freezing behaviors caused by the 2-MT (*Figure 4D−E*). Besides the 2-MT, footshock is another standard paradigm that induces robust freezing behaviors. The percentage of the freezing behaviors was increased in both groups as the footshock repeated, but this process was slowed down in the NpHR3.0 group compared with the control group (*Figure 4F−G*).

We also examined whether inhibition of the PVT-projecting PBN neurons is sufficient to rescue aversion. We placed the 2-MT in one chamber to induce the conditioned place aversion and constantly delivered the 589 nm laser (*Figure 4H*). The NpHR3.0 group mice spent more time on the 2-MT paired chamber compared with control group mice (*Figure 4I−J*), suggesting that inhibition of the PBN-PVT pathway could reduce the aversion induced by the 2-MT. Furthermore, the moving duration in this behavioral test was increased than that of the control group (*Figure 4K*), consistent with the result that inhibition of PBN-PVT projection would partially rescue the freezing fear-behavior induced by the 2-MT (*Figure 4E*).

The PVT_{PBN} neurons are activated by the 2-MT and footshock

By using *in vivo* fiber photometry, we found the calcium signals of the PVT neurons were increased after footshock and air-puff stimuli (*Figure 5A−F*), indicating that the calcium signals of the PVT neurons could be increased by noxious and aversive stimulation. Besides, we injected the AAV2/1-hSyn-Cre virus into the PBN of *Rosa26-tdTomato* mice (*Figure 5G*), which could anterogradely label the neurons innervated by the PBN with Cre recombinase

(Zingg et al., 2017). The distribution pattern of tdTomato$^+$ neurons in PVT (hereafter referred to as PVT_{PBN} neurons) was shown in *Figure 5H−J*. The other brain areas that received projections from the PBN nucleus were represented in *Figure5−figure supplement 1A−J*. We used Fos as a marker to assess the neuronal activity change in 2-MT or footshock treated mice. The percentage of Fos$^+$tdTomato$^+$ neurons/tdTomato$^+$ neurons in the PVT was significantly increased in the aversive stimuli-treated mice than that of control mice (*Figure 5K−N*), confirming that the PVT_{PBN} neurons could be activated by aversive stimuli. These results support the notion that the PVT neurons innervated by the PBN are involved in processing negative experiences.

Pharmacogenetics activation of the PVT_{PBN} neurons induces anxiety-like behaviors

To further investigate the specific role PVT_{PBN} neurons play in modulating negative emotions, the AAV2/1-hSyn-Cre virus was injected into the bilateral PBN, and the AAV2/9-hSyn-DIO-hM3Dq-mCherry virus or control virus was injected into the PVT to activate the PVT_{PBN} neurons specifically (Figure 6A). The majority of the PVT_{PBN} neurons could be activated by CNO in the hM3Dq expressing mice but not the control mice (*Figure 6B−D*). We found that pharmacogenetics activation of the PVT_{PBN} neurons reduced the center time (*Figure 6E−F*), but did not affect the unmoving time, the total distance, and the velocity in the OFT (data not shown). Similarly, the time spent in open quadrants was decreased in the EZM test in hM3Dq expressing mice (*Figure 6G−H*). And the unmoving time in the EZM test had an increased tendency in hM3Dq expressing mice (*Figure 6I*). We did not observe obvious nociception-related behaviors, such as forelimb wiping, hindlimb flinching, licking, or bitting during the experiments. These results indicate pharmacogenetics activation of PVT_{PBN} neurons induces anxiety-like behaviors.

Furthermore, we examined the anatomic distribution of terminals of

PVT_{PBN} neurons. We labeled the PVT_{PBN} neurons in WT mice by injecting the AAV2/1-hSyn-Cre virus into the PBN and AAV2/8-EF1a-DIO-EGFP virus into the PVT (*Figure6−figure supplement 1A*). We found that the PVT_{PBN} neurons sent projections to several brain areas, in particular the accumbens nucleus core (NAc), the bed nucleus of the stria terminalis (BNST), and CeA (*Figure6−figure supplement 1B−H*), which was similar to the early tracing research of PVT efferent projections *(Kirouac, 2015)*.

Discussion

In this study, we employed viral tracing and electrophysiology to confirm the monosynaptic excitatory connectivity between the PBN and the PVT nuclei. Optogenetics or pharmacogenetics activation of the PBN-PVT projection or the PVT-projecting PBN neurons induced anxiety-like and fear-like behaviors. Optogenetics inhibition of the PVT-projecting PBN neurons could partially rescue 2-MT induced fear-like and aversion-like behaviors as well as footshock-induced freezing behaviors. Besides, the PVT_{PBN} neurons were involved in negative experiences processing and activation of these neurons induced anxiety-like behaviors. Together, our results reveal the functional role of the PBN-PVT projection in modulating negative emotions in mice.

PBN efferents and PBN-PVT monosynaptic excitatory projection

The PBN is a critical hub receiving sensory information from the spinal cord *(Todd, 2010)*. The widespread distribution of PBN efferents contributes to different aspects of behavioral and physiological responses. Previous studies showed that the CGRP-expressing neurons in the PBN project to the CeA contribute to the affective dimension of pain. In contrast, non-CGRP neurons may transmit sensory pain information *(Han et al., 2015)*. The projections from lateral PBN to the VMH or PAG are involved in producing escape behaviors to avoid injury, while the projections from the IPBN to the BNST or the CeA participate in facilitating aversive memory *(Chiang et al., 2020)*. The PBN

neurons, which receive projections from the spinal cord, form strong functional synaptic connections with the intralaminar thalamic nucleus but not the CeA neurons to process the nociceptive signals *(Deng et al., 2020)*. The PVT nucleus located in the middle line of the brain is an important area that participates in affection processing *(Kirouac, 2015)*. Although recent research has reported the projecting fibers from PBN were found in the PVT *(Chiang et al., 2020)*, remarkably little is known about the connectivity information and function of the PBN-PVT projection. Our tracing results showed that the PVT received dense projections from the PBN, which is consistent with the previous study *(Chiang et al., 2020)*. Moreover, the electrophysiologic results confirmed that the PBN-PVT projection is a monosynaptic excitatory connection and the PVT neurons have relatively high connectivity with the PBN neurons.

PBN-PVT projection modulates negative emotion

We found that activation of PBN projections in the PVT or the PVT-projecting PBN neurons induced anxiety-like behaviors and fear-like behaviors in the OFT and EZM. In the RTPA test, the aversion appeared when the laser was on and disappeared when the laser was off, indicating the aversion was transient and could not be translated to associative learning. It was further confirmed by the cue-dependent optogenetics conditioning test. Selectively optogenetics inhibition of PVT-projecting PBN neurons could relieve the fear- and aversion-like behaviors induced by aversive stimuli, such as 2-MT and footshock, indicating that the PBN-PVT projection is necessary for modulating negative emotions. Our calcium imaging and Fos staining results indicated PVT neurons were activated after exposure to some negative stimuli, consistent with a previous study *(Zhu et al., 2018)*. The activation of PBN innervated PVT neurons induced anxiety-like behaviors, suggesting the PVT neurons conveyed the information from the PBN is involved in modulating negative emotions.

Some studies have reported that activation of the PBN-CeA pathway is

sufficient to drive a series of negative emotion-related behaviors *(Bowen et al., 2020; Cai et al., 2018; Han et al., 2015)*, enable associative learning, and generate aversive memory *(Chiang et al., 2020)*. Distinct from the PBN-CeA projection, activation of the PBN-PVT only induced transient negative emotion-related behaviors. There was a study that reported that only a few Fluoro-gold (FG)/tetramethylrhodamine-dextran (TMR) double-labeled neurons were sparsely distributed in the PBN of the mice injected with FG into the PVT and TMR into the CeA *(Liang et al., 2016)*. Our results showed few collateral projecting axons in the CeA from the PVT-projecting PBN neurons. These results suggested the PBN-PVT pathway and the PBN-CeA pathway are two parallel pathways originating from distinct efferent neurons within the PBN to perform distinct functions.

The potential role of PBN-PVT projection in depression and pain

It's worth noting that although the pharmacogenetics activation of the PVT-projecting PBN neurons induced anxiety-like behaviors and fear-like behaviors in the hM3Dq group mice, no depression-like symptoms were observed in TST and FST. On the other side, chronic pain models, such as the partial sciatic nerve ligation model, the spared nerve injury model, and complete Freund's adjuvant model, generally induce anxiety and depression at least 3-4 weeks after the surgery in mice *(Dimitrov et al., 2014; Zhou et al., 2019)*. Our study collected the behavioral data 30 minutes after a single dose of CNO injection. Different behavioral tests were performed at least three days apart to eliminate the residual CNO effects. We hypothesized that depression-like behaviors might be observed if we repeatedly activate the PBN-PVT projection for weeks. However, whether the PBN-PVT is involved in depression is still unknown.

A recent study revealed that the PBN neurons convey nociception information from the spinal cord to the ILN, which is relatively closed to the PVT *(Deng et al., 2020)*. In our results, pharmacogenetics activation of

PVT-projecting PBN neurons did not affect the basal nociceptive thresholds or formalin-induced licking behaviors. Moreover, no obvious nociception-related behaviors (such as forelimb wiping, hindlimb flinching, licking, or biting) were found through specific manipulation of the PBN innervated PVT neurons, which suggests that the PBN-PVT projection might be not involved in nociceptive information processing.

The tracing results showed the PVT_{PBN} neurons projected to multiple brain areas, particularly the NAc, the BNST, and the CeA. The BNST and the CeA have been previously implicated in anxiety-like behaviors *(Jennings et al., 2013; Tye et al., 2011)*. A study also found that PVT mediates descending pain facilitation underlying persistent pain conditions via the PVT-CeA-PAG circuit *(Liang et al., 2020)*. The specific functional roles of different projections of PVT_{PBN} neurons need further examination.

In summary, we dissected a novel PBN downstream projection target and identified the significant role of the PBN-PVT projection in modulating negative emotions. Thus, our study paves the way for further examining the functional role of the PBN-PVT neural circuit in modulating the affections.

Acknowledgements

We thank Dr. Hua-Tai Xu for providing *Rosa26-tdTomato* mice. We thank Dr. Yan-Gang Sun for providing *VgluT2-ires-Cre* mice. We thank all the lab members of D.M. for their helpful discussion. This work was supported by the National Natural Science Foundation of China (No. 31900717), the Shanghai Sailing Program (19YF1438700 to D.M.), the Young Elite Scientists Sponsorship Program of China Association for Science and Technology (2019QNRC001 To D.M.), and the Starting Research Fund from the Shanghai General Hospital.

Author contributions

Y.B.Z. performed the virus injection experiments and behavioral experiments.

R.Z. performed the electrophysiological experiments. Y.B.Z., Y.W., and P.F.L. performed the histological experiments. Y.B.Z., J.B.L., and D.M. designed the experiments. Y.B.Z. and D.M. wrote the manuscript.

Materials and methods

Animals

Male C57Bl/6J wild-type mice, *Rosa26-tdTomato* mice (gifted from Dr. Hua-Tai Xu, Institutes of Neuroscience, Chinese Academic of Sciences), *VgluT2-ires-Cre* mice (gifted from Dr. Yan-Gang Sun, Institutes of Neuroscience, Chinese Academic of Sciences) were used. Animals were housed in standard laboratory cages in a temperature (23-25°C)-controlled vivarium with a 12:12 light/dark cycle, free to food and water. For tracing and behavioral experiments, the mice were injected with the virus at 7−8 weeks old and performed the behavioral tests at 11−12 weeks old. For the electrophysiological experiments, the mice were injected with the virus at 4−6 weeks old to accomplish the electrophysiological experiments at 7−9 weeks old. For *in vivo* fiber photometry experiments, the mice were injected with the virus at 7−8 weeks old to accomplish the experiments at 10−11 weeks old. All animal experiment procedures were approved by the Animal Care and Use Committee of the Animal Care and Use Committee of Shanghai General Hospital.

Stereotaxic surgery

Mice were anesthetized by vaporized sevoflurane (induction, 3%; maintenance, 1.5%) and head-fixed in a mouse stereotaxic apparatus (RWD Life Science Co.). For tracing studies, the AAV2/8-EF1a-DIO-EGFP virus (300 nl, S0270, Taitool Bioscience) was injected into the PBN of *VgluT2-ires-Cre* mice in the stereotaxic coordinate: anteroposterior (AP) −5.2 mm, mediolateral (ML) +1.3 mm, and dorsoventral (DV) −3.4 mm.

For electrophysiological experiments, the AAV2/8-hSyn-ChR2-mCherry virus (300 nl, 4 x 10^{12} v.g./ml, AG26976, Obio Technology) was injected into the PBN nucleus of WT mice.

For the retrovirus injection surgery, the retrograde transport Cre recombinase retroAAV2/2-hSyn-Cre virus (150 nl, 4 x 10^{12} v.g./ml,

S0278-2RP-H20, Taitool Bioscience) was injected in the *Rosa26-tdTomato* mice at two locations of PVT respectively: (1) AP −1.22 mm, ML 0 mm, DV −2.9 mm; (2) AP −1.46 mm, ML 0 mm, DV −2.9 mm.

For optogenetics activation of PVT-projecting PBN fibers, the AAV2/9-EF1a-DIO-ChR2-mCherry virus (300 nl, 4 x 10^{12} v.g./ml, AAV2/9-S0170, Taitool Bioscience) or the AAV2/9-EF1a-DIO-mCherry virus (300 nl, 4 x 10^{12} v.g./ml, AG20299, Obio Technology) were bilaterally injected into the PBN (mentioned above) of *VgluT2-ires-Cre* mice, and a 200 μm diameter optic fiber was implanted over the PVT with a 20° angle towards the midline.

For the pharmacogenetics activation of PVT-projecting PBN neurons, the retroAAV2/2-hSyn-Cre virus (150 nl, 4 x 10^{12} v.g./ml, S0278-2RP-H20, Taitool Bioscience) was injected into the PVT (mentioned above), the AAV2/9-hSyn-DIO-hM3Dq-mCherry virus (300 nl, 4 x 10^{12} v.g./ml, PT-0019, BrainVTA) or the control AAV2/9-EF1a-DIO-mCherry virus were bilateral injected into the PBN (AP −5.2 mm, ML ±1.3 mm, DV −3.4 mm) of the WT mice.

For optogenetics inhibition of PVT-projecting PBN neurons, retroAAV2/2-hSyn-Cre was injected into the PVT, AAV2/9-EF1a-DIO-NpHR3.0-EYFP virus (300 nl, 4 x 10^{12} v.g./ml, AG26966, Obio Technology) or the AAV2/8-EF1a-DIO-EGFP virus was injected into the PBN of WT mice, the left optic fiber was implanted over the PBN (AP −5.2 mm, ML +1.3 mm, DV −3.4) vertically and the right one were placed over the PBN with a 20° angle towards the midline.

For *in vivo* fiber photometry experiments, the AAV2/8-hSyn-GCaMP6s virus (200 nl, 4 x 10^{12} v.g./ml, S0225-8, Taitool Bioscience) was injected into the PVT nucleus (AP −1.46 mm, ML 0 mm, DV −2.90 mm) of the WT mice, the optic fiber was implanted above the PVT with a 20° angle towards the midline.

For pharmacogenetics activation of PVT_{PBN} neurons, the AAV2/1-hSyn-Cre virus (300 nl, 1.5 x 10^{13} v.g./ml, S0278-1-H50, Taitool

Bioscience) was bilaterally injected into the PBN nucleus, the AAV2/9-hSyn-DIO-hM3Dq-mCherry virus or the control AAV2/9-EF1a-DIO-mCherry virus was injected into the PVT of the WT mice.

The virus was infused through a glass pipette (10−20 μm in diameter at the tip) at the rate of 50−100 nl/minute. The injection pipette was left in place for additional 8 minutes. After the surgeries, the skin was closed by the sutures, and the optic fiber was secured through the dental acrylic. Generally, tracing, electrophysiological or behavioral experiments were performed at least three weeks later. After experiments, histological analysis was used to verify the location of viral transduction and the optic fiber. The mice without correct transduction of virus and right site of optic fiber were excluded for analysis.

Fos induction

The mice were habituated for three days and performed gentle grabbing and holding for 1 minute, five times every day in their home cages to minimize background Fos expression.

To study the effect of pharmacogenetics manipulations on PVT-projecting PBN neurons, we injected (i.p.) 0.5 mg/kg clozapine N-oxide (CNO, Sigma). Ninety minutes later, the brain tissues were processed.

To assess 2-MT evoked Fos expression in the PVT, the mice were closed into a chamber with a floor covered with cotton contained 100 ml, 1:1000 2-MT volatilized the predator odor for 90 minutes.

To assess shock stimuli induced Fos expression in the PVT, we placed the mice into the chamber and delivered 30 times inevitable footshock (0.5 mA, 1 second) with a variable interval (averaging 59 seconds). After stimulation, animals were kept in the same apparatus for another 60 minutes, and brain tissues were then processed.

Histology

Animals were deeply anesthetized with vaporized sevoflurane and transcardially perfused with 20 ml saline, followed by 20 ml paraformaldehyde (PFA, 4% in PBS). Brains were extracted and soaked in 4% PFA at 4°C for a

minimum of 4 hours and subsequently cryoprotected by transferring to a 30% sucrose solution (4°C, dissolved in PBS) until brains were saturated (for 36−48 hours). Coronal brain sections (40 μm) were cut using a freezing microtome (CM1950, Leica). The slices were collected and stored in PBS at 4°C until immunohistochemical processing. Nuclei were stained with DAPI (Beyotime, 1:10000) and washed three times with PBS.

The brain sections undergoing immunohistochemical staining were washed in PBS 3 times (10 minutes each time) and incubated in a blocking solution containing 0.3% TritonX-100 and 5% normal donkey serum (Jackson ImmunoResearch, USA) in PBS for 1 hour at 37°C. Sections were then incubated (4°C, 24 hours) with primary antibodies anti-rabbit Fos (1:4000, ab190289, Abcam) dissolved in 1% normal donkey serum solution. Afterward, sections were washed in PBS 4 times (15 minutes each time), then incubated with secondary antibodies Alexa Flour 488 conjugated donkey anti-rabbit IgG (1:800, Jackson) for 2 hours at room temperature. After DAPI staining and washing with PBS, sections were mounted on glass microscope slides, dried, and covered with 50% glycerin (ThermoFisher). The photofluorograms were taken by the Leica DMi8 microscope, and the confocal images were acquired with the Leica SP8 confocal microscopy. The photomicrographs were further processed by Fiji and Photoshop.

Quantification of the neurons and fiber intensity

The number of retrogradely labeled neurons from the PVT nucleus and the anterogradely labeled neurons from the PBN nucleus of *Rosa26-tdTomato* mice was quantified across every other 40 μm coronal section. The numbers of labeled cells in each ROI (400 x 400 pixels) of each brain region were manually counted by using Fiji.

For quantification of fluorescence of PVT_{PBN} efferents, the downstream targets of PVT_{PBN} neurons were taken photofluorograms with identical exposure time, the mean fluorescence value in each ROI (400 x 400 pixels) of each brain region was analyzed by Fiji. The fiber intensity was calculated as

the fluorescence value of each brain region divided by that of the NAc.

All data came from three different mice and were presented as mean ± SEM.

Electrophysiology

The electrophysiological experiment was performed as previously described *(Mu et al., 2017)*. Mice were anesthetized with sevoflurane and perfused by the ice-cold solution containing (in mM) sucrose 213, KCl 2.5, NaH_2PO_4 1.25, $MgSO_4$ 10, $CaCl_2$ 0.5, $NaHCO_3$ 26, glucose 11 (300−305 mOsm). Brains were quickly dissected, and the coronal slice (250 μm) containing the PBN or PVT were chilled in ice-cold dissection buffer using a vibratome (V1200S, Leica) at a speed of 0.12 mm/second. The coronal sections were subsequently transferred to a chamber and incubated in the artificial cerebrospinal fluid (ACSF, 34°C) containing (in mM): NaCl 126, KCl 2.5, NaH_2PO_4 1.25, $MgCl_2$ 2, $CaCl_2$ 2, $NaHCO_3$ 26, glucose 10 (300−305 mOsm) to recover for at least 40 minutes, then kept at room temperature before recording. All solutions were continuously bubbled with 95% O_2/5% CO_2.

All experiments were performed at near-physiological temperatures (30−32°C) using an in-line heater (Warner Instruments) while perfusing the recording chamber with ACSF at 3 ml/minute using a pump (HL-1, Shanghai Huxi). Whole-cell patch-clamp recordings were made from the target neurons under IR-DIC visualization and a CCD camera (Retiga ELECTRO, QIMAGING) using a fluorescent Olympus BX51WI microscope. Recording pipettes (2−5 MΩ; Borosilicate Glass BF 150-86-10; Sutter Instrument) were prepared by a micropipette puller (P97; Sutter Instrument) and backfilled with potassium-based internal solution containing (in mM) K-gluconate 130, $MgCl_2$ 1, $CaCl_2$ 1, KCl 1, HEPES 10, EGTA 11, Mg-ATP 2, Na-GTP 0.3 (pH 7.3, 290 mOsm) or cesium-based internal solution contained (in mM) $CsMeSO_3$ 130, $MgCl_2$ 1, $CaCl_2$ 1, HEPES 10, QX-314 2, EGTA 11, Mg-ATP 2, Na-GTP 0.3 (pH 7.3, 295 mOsm). Biocytin (0.2%) was included in the internal solution.

In PBN-PVT ChR2 experiments, whole-cell recordings of PBN neurons

with current-clamp (I = 0 pA) were obtained with pipettes filled with the potassium-based internal solution. The 473 nm laser (5 Hz, 10 Hz, 20 Hz pulses, 0.5 ms duration, 2 mW/mm^2) was used to activate PBN ChR2 positive neurons. Light-evoked EPSCs of PVT neurons recorded with voltage-clamp (holding voltage of -70 mV) were obtained with pipettes filled with the cesium-based internal solution. The 473 nm laser (20 Hz paired pulses, 1 ms duration, 4 mW/mm^2) was used to activate ChR2 positive fibers. The light-evoked EPSCs were completely blocked by 1 μM TTX (tetrodotoxin), rescued by 100 μM 4-AP (4-Aminopyridine), and blocked by 10 μM NBQX (6-nitro-7-sulphamoylbenzo(f)quinoxaline-2,3-dione). NBQX and TTX were purchased from Tocris Bioscience. All other chemicals were obtained from Sigma.

Voltage-clamp and current-clamp recordings were carried out using a computer-controlled amplifier (MultiClamp 700B; Molecular Devices, USA). During recordings, traces were low-pass filtered at 4 kHz and digitized at 10 kHz (DigiData 1550B1; Molecular Devices). Data were acquired by Clampex 10.6 and filtered using a low-pass-Gaussian algorithm (-3 dB cut-off frequency = 1000 Hz) in Clampfit 10.6 (Molecular Devices).

Optogenetics manipulation

For activating the PBN-PVT projection, a 473 nm laser (20 Hz, 5 ms pulse duration, 5 mW) was delivered. For inhibition of the PVT-projecting PBN neurons, a constant laser (589 nm, 10 mW) was delivered.

Pharmacogenetics manipulation

All behavioral tests were performed 30 minutes after intraperitoneal (i.p.) injection of 0.5 mg/kg CNO in pharmacogenetics manipulation. Different behavior tests were performed at least three days apart.

Open field test

The open field test (OFT) was used to assess locomotor activity and anxiety-related behavior in an open field arena (40 x 40 x 60 cm) with opaque plexiglass walls. The mouse was placed in the center of the box and recorded

by a camera attached to a computer. The movement was automatically tracked and analyzed by AniLab software (Ningbo AnLai, China). The total distance traveled, the total velocity, the total unmoving time (the mice were considered to be unmoving if unmoving time lasts more than 1 s), and time spent in the center area (20 x 20 cm) were measured. The box was cleaned with 70% ethanol after each trial.

To assess the effect of optogenetics activation of the PBN-PVT projection, 15 minutes session consisting of 5 minutes pre-test (laser OFF), 5 minutes laser ON-test, and 5 minutes post-test (laser OFF) periods. Laser (473 nm, 20 Hz, 5 ms, 5 mW) was delivered during the light on phase.

To assess the effect of pharmacogenetics manipulations of PVT-projecting PBN neurons on locomotor activity and emotion, we recorded the mice's movement for 10 minutes, 30 minutes after intraperitoneal (i.p.) injection with clozapine N-oxide (CNO, 0.5 mg/ kg, Sigma).

To assess whether optogenetics inhibition of the PVT-projecting PBN neurons had an effect on locomotor activity and emotion, we delivered a constant laser (589 nm, 10 mW) during the laser ON period (5−10 minutes), the laser was off during the 0−5 minutes and the 10−15 minutes.

Real-time place aversion (RTPA) test

Mice were habituated on day 1 to a custom-made 20 x 30 x 40 cm two-chamber apparatus (distinct wall colors and stripe patterns). Each mouse was placed in the center and allowed to explore both chambers without laser stimulation for 10 minutes on day 2. The movement was recorded for 10 minutes as a baseline. The mice performed a slight preference for the black chamber according to the fact the mice have innate aversive to brightly illuminated areas. On day 3, 473 nm laser stimulation (20 Hz, 5 ms, 5 mW) was automatically delivered when the mouse entered or stayed in the black chamber and turned off when the mouse exited the black chamber for 10 minutes. Finally, the mouse was allowed to freely explore both chambers without laser stimulation for another 10 minutes. The RTPA location plots and

total time on the stimulated side were recorded and counted with the AniLab software.

To assess the effect of optogenetics inhibition of the PVT-projecting PBN neurons on the aversive emotion induced by 2-methyl-2-thiazoline (2-MT). Three cotton balls contained 5 ml 1:1000 2-MT solution were placed on the black chamber to induced fear-odor, then a constant laser (589 nm, 10 mW) was delivered during the 10 minutes test.

Cue-dependent optogenetics conditioning

Video Freeze fear conditioning system with modified top to accommodate optogenetics equipment (MED Associates, MED-VFC-OPTO-USB-M) and Video Freeze software were used.

On the 1st day: mice were habituated to the fear conditioning chambers and allowed to explore for 2 minutes freely, then three tones (75 dB, 4 kHz, 30 seconds duration) separated by a variable interval with a range of 60−120 seconds and the average of 90 seconds were delivered.

On the 2nd day: mice were trained with the sound cue (75 dB, 4 kHz, 30 seconds) paired with a simultaneous 30 seconds laser pulse train (20 Hz, 5 ms, 5 mW) for six times separated by a variable interval (averaging 90 seconds). The mice were kept in the conditioning chamber for another 60 seconds before being returned to the home cages.

After 24 hours, mice were placed back into the original training chamber for 3 minutes to do the contextual test. After 2−3 hours, the conditioning chamber was modified by changing its metal floor and sidewalls. Mice were placed in the altered chamber for 3 minutes to measure the freezing level in the altered context. A tone (75 dB, 4 kHz) was delivered for 30 seconds to perform the cue test.

The behavior of the mice was recorded and analyzed with the Video Freeze software. Freezing was defined as the complete absence of movement for at least 0.5 seconds. On the conditioning day, the freezing percentages in the 30 seconds after each tone were summarized. The chamber was cleaned

with 70% ethanol after each trial.

Freezing behavior

For analyses of freezing behavior induced by pharmacogenetics activation of PVT-projecting PBN neurons, we injected CNO and recorded the mouse behavior using the Video Freeze fear conditioning system (MED Associates, MED-VFC-OPTO-USB-M) 30 minutes later.

The Video Freeze fear conditioning system was also used to assess the effect of optogenetics inhibition of the PVT-projecting PBN neurons on the fear-like behavior induced by 2-methyl-2-thiazoline (2-MT, Sigma). 100 ml 1:1000 2-MT dissolved in the ddH_2O was soaked into the cotton lay on the button of the training box. Constant laser (589 nm, 10 mW) was delivered during the tests (10 minutes).

The Video Freeze fear conditioning system (MED Associates, MED-VFC-OPTO-USB-M) was also used to assess the freezing behavior induced by footshock. After free exploration of the chamber for 2 minutes, 15 times footshocks (0.5 mA,1 second) were delivered with an interval of 59 seconds. The 10 mW 589 nm laser was constantly delivered for 15 minutes. The freezing percentages in 30 seconds after each shock were analyzed.

Elevated zero maze (EZM)

The EZM was an opaque plastic circle (60 cm diameter), which consisted of four sections with two opened and two closed quadrants. Each quadrant had a path width of 6 cm. The maze was elevated 50 cm above the floor. The animals were placed into an open section facing a closed quadrant and freely explore the maze for 5 minutes.

Tail suspension test (TST)

Mice were individually suspended by an adhesive tape placed roughly 2 cm from the tip of the tail and videotaped for 6 minutes. Mice were considered immobile without initiated movements, and the immobility time was scored in the last 3 minutes by an observer unknown of the treatments.

Forced swim test (FST)

Mice were individually placed for 6 minutes in clear cylinders (45 cm height, 20 cm internal diameter) containing freshwater (25°C, 15 cm depth). The swimming activity was videotaped, and immobility time in the last 3 minutes was counted manually by an investigator unaware of animal grouping. The mice were considered immobile when they stopped swimming, struggling, or only slightly moved to keep the nose above the surface.

Von Frey test

The Von Frey test was used to assess the mechanical sensitivity. The mice were acclimated to the observation chambers for two days (2 hours for each day) before the test. A series of von Frey hairs with logarithmically incrementing stiffness (0.16−2.0 grams) were used to perpendicularly stimulate the mouse hind paw. The 50% paw withdrawal threshold was determined using the up-down method.

Hargreaves test

Hargreaves tests were performed as described previously *(Mu et al., 2017)*. Mice were placed in an individual plexiglass box with a glass floor. A radiant heat beam was exposed directly to the hind paw until the paw was withdrawn. The trials were repeated three times with an interval of at least 15 minutes. To avoid tissue damage, the test was executed with a 20 seconds cut-off time.

Formalin test

In the formalin test, the mice received an intraplantar injection of formalin (5%, 20 μl/mouse), then were immediately placed into a plexiglass box (width: 10 cm, length: 10 cm, height: 15 cm) individually to record the pain-related licking behaviors for 1 hour. All videos were analyzed by trained investigators blinded to the experimental treatment of the animals.

Rotarod test

Mice were trained twice on a rotarod apparatus (MED Associates) with a rod accelerated 5−20 revolutions per minute (r.p.m.) for 5 minutes before the experimental day. On the second day, each mouse underwent three trials with a rod was programmed to accelerate from 0 to 40 rpm over 300 seconds, then

the average rpm at the point of falling was recorded.

Fiber photometry

In vivo fiber photometry experiments were performed as previously described *(Zhu et al., 2020)*. After two weeks for virus expression, the mice were gently handled to be familiar with the calcium signal recording experiments (Thinker-Biotech). A TTL signal (for synchronization) was manually tagged with the shock and air puff to evaluate the activity of PVT neurons. The calcium transient was recorded at 50 Hz. The fluorescence values change (ΔF/F) was calculated from the formula of (F−F0)/F0 and the F0 represented the median of the fluorescence values in the baseline period (−1 to −0.5 seconds relative to the stimulation onset). To precisely quantified the change of the fluorescence values across the shock or air-puff stimulation, we defined 0.5−1.0 seconds after the onset as the post-stimulus period.

Analysis

Statistical detection methods include unpaired student's *t*-test, paired student's *t*-test, two-way ANOVA with Bonferroni's correction for multiple comparisons. A value of $p < 0.05$ was considered statistically significant. All data were represented as mean ± SEM.

REFERENCES

Armbruster BN, Li X, Pausch MH, Herlitze S, Roth BL. (2007). Evolving the lock to fit the key to create a family of G protein-coupled receptors potently activated by an inert ligand. *PNAS,* **104**:5163-5168. DOI: https://doi.org/10.1073/pnas.0700293104, PMID:17360345

Beas BS, Wright BJ, Skirzewski M, Leng Y, Hyun JH, Koita O, Ringelberg N, Kwon HB, Buonanno A, Penzo MA. (2018). The locus coeruleus drives disinhibition in the midline thalamus via a dopaminergic mechanism. *Nature Neuroscience,* **21**:963-973. DOI: https://doi.org/10.1038/s41593-018-0167-4, PMID:29915192

Bowen AJ, Chen JY, Huang YW, Baertsch NA, Park S, Palmiter RD. (2020).

Dissociable control of unconditioned responses and associative fear learning by parabrachial CGRP neurons. *eLife,* **9**. DOI: https://doi.org/10.7554/eLife.59799, PMID:32856589

Cai YQ, Wang W, Paulucci-Holthauzen A, Pan ZZ. (2018). Brain circuits mediating opposing effects on emotion and pain. *Journal of Neuroscience,* **38**:6340-6349. DOI: https://doi.org/10.1523/JNEUROSCI.2780-17.2018, PMID:29941444

Campos CA, Bowen AJ, Roman CW, Palmiter RD. (2018). Encoding of danger by parabrachial CGRP neurons. *Nature,* **555**:617-622. DOI: https://doi.org/10.1038/nature25511, PMID:29562230

Chiang MC, Bowen A, Schier LA, Tupone D, Uddin O, Heinricher MM. (2019). Parabrachial complex: a hub for pain and aversion. *Journal of Neuroscience,* **39**:8225-8230. DOI: https://doi.org/10.1523/JNEUROSCI.1162-19.2019, PMID:31619491

Chiang MC, Nguyen EK, Canto-Bustos M, Papale AE, Oswald AM, Ross SE. (2020). Divergent neural pathways emanating from the lateral parabrachial nucleus mediate distinct components of the pain response. *Neuron,* **106**:927-939. DOI: https://doi.org/10.1016/j.neuron.2020.03.014, PMID:32289251

Deng J, Zhou H, Lin JK, Wei YC, Xu XH, Sun YG. (2020). The parabrachial nucleus directly channels spinal nociceptive signals to the intralaminar thalamic nuclei, but not the amygdala. *Neuron,* **107**:909-923. DOI: https://doi.org/10.1016/j.neuron.2020.06.017, PMID:32649865

Dimitrov EL, Tsuda MC, Cameron HA, Usdin TB. (2014). Anxiety- and depression-like behavior and impaired neurogenesis evoked by peripheral neuropathy persist following resolution of prolonged tactile hypersensitivity. *Journal of neuroscience,* **34**:12304-12312. DOI: https://doi.org/10.1523/JNEUROSCI.0312-14.2014, PMID:25209272

Do-Monte FH, Quinones-Laracuente K, Quirk GJ. (2015). A temporal shift in the circuits mediating retrieval of fear memory. *Nature,* **519**:460-463. DOI:

https://doi.org/10.1038/nature14030, PMID:25600268

Han S, Soleiman MT, Soden ME, Zweifel LS, Palmiter RD. (2015). Elucidating an affective pain circuit that creates a threat memory. *Cell,* **162**:363-374. DOI: https://doi.org/10.1016/j.cell.2015.05.057, PMID:26186190

Hsu DT, Kirouac GJ, Zubieta JK, Bhatnagar S. (2014). Contributions of the paraventricular thalamic nucleus in the regulation of stress, motivation, and mood. *Frontiers in Behavioral Neuroscience,* **8**:73. DOI: https://doi.org/10.3389/fnbeh.2014.00073, PMID:24653686

Huang TW, Lin SH, Malewicz NM, Zhang Y, Zhang Y, Goulding M, LaMotte RH, Ma QF. (2019). Identifying the pathways required for coping behaviours associated with sustained pain. *Nature,* **565**:86-90. DOI: https://doi.org/10.1038/s41586-018-0793-8, PMID:30532001

Isosaka T, Matsuo T, Yamaguchi T, Funabiki K, Nakanishi S, Kobayakawa R, Kobayakawa K. (2015). Htr2a-expressing cells in the central amygdala control the hierarchy between innate and learned fear. *Cell,* **163**:1153-1164. DOI: https://doi.org/10.1016/j.cell.2015.10.047, PMID:26590419

Jennings JH, Sparta DR, Stamatakis AM, Ung RL, Pleil KE, Kash TL, Stuber GD. (2013). Distinct extended amygdala circuits for divergent motivational states. *Nature,* **496**:224-228. DOI: https://doi.org/10.1038/nature12041, PMID:23515155

Jimenez JC, Su K, Goldberg AR, Luna VM, Biane JS, Ordek G, Zhou P, Ong SK, Wright MA, Zweifel L, Paninski L, Hen R, Kheirbek MA. (2018). Anxiety cells in a hippocampal-hypothalamic circuit. *Neuron,* **97**:670-683. DOI: https://doi.org/10.1016/j.neuron.2018.01.016, PMID:29397273

Kaur S, Pedersen NP, Yokota S, Hur EE, Fuller PM, Lazarus M, Chamberlin NL, Saper CB. (2013). Glutamatergic Signaling from the Parabrachial Nucleus Plays a Critical Role in Hypercapnic Arousal. *Journal of Neuroscience,* **33**:7627-7640. DOI: https://doi.org/10.1523/Jneurosci.0173-13.2013, PMID:WOS:000318420400003

Kirouac GJ. (2015). Placing the paraventricular nucleus of the thalamus within the brain circuits that control behavior. *Neuroscience and Biobehavioral Reviews,* **56**:315-329. DOI: https://doi.org/10.1016/j.neubiorev.2015.08.005, PMID:26255593

Li S, Kirouac GJ. (2012). Sources of inputs to the anterior and posterior aspects of the paraventricular nucleus of the thalamus. *Brain Structure & Function,* **217**:257-273. DOI: https://doi.org/10.1007/s00429-011-0360-7, PMID:22086160

Liang SH, Yin JB, Sun Y, Bai Y, Zhou KX, Zhao WJ, Wang W, Dong YL, Li YQ. (2016). Collateral projections from the lateral parabrachial nucleus to the paraventricular thalamic nucleus and the central amygdaloid nucleus in the rat. *Neuroscience Letters,* **629**:245-250. DOI: https://doi.org/10.1016/j.neulet.2016.07.017, PMID:27423318

Liang SH, Zhao WJ, Yin JB, Chen YB, Li JN, Feng B, Lu YC, Wang J, Dong YL, Li YQ. (2020). A neural circuit from thalamic paraventricular nucleus to central amygdala for the facilitation of neuropathic pain. *Journal of Neuroscience,* **40**:7837-7854. DOI: https://doi.org/10.1523/JNEUROSCI.2487-19.2020, PMID:32958568

Mu D, Deng J, Liu KF, Wu ZY, Shi YF, Guo WM, Mao QQ, Liu XJ, Li H, Sun YG. (2017). A central neural circuit for itch sensation. *Science,* **357**:695-699. DOI: https://doi.org/10.1126/science.aaf4918, PMID:28818946

Öhman A, Mineka S. (2001). Fears, phobias, and preparedness: Toward an evolved module of fear and fear learning. *Psychological Review,* **108**:483-522. DOI: https://doi.org/10.1037/0033-295x.108.3.483, PMID:11488376

Palmiter RD. (2018). The parabrachial nucleus: CGRP neurons function as a general alarm. *Trends in Neurosciences,* **41**:280-293. DOI: https://doi.org/10.1016/j.tins.2018.03.007, PMID:29703377

Penzo MA, Robert V, Tucciarone J, De Bundel D, Wang M, Van Aelst L, Darvas M, Parada LF, Palmiter RD, He M, Huang ZJ, Li B. (2015). The paraventricular thalamus controls a central amygdala fear circuit. *Nature,*

519:455-459. DOI: https://doi.org/10.1038/nature13978, PMID:25600269

Ren SC, Wang YL, Yue FG, Cheng XF, Dang RZ, Qiao QC, Sun XQ, Li X, Jiang Q, Yao JW, Qin H, Wang GZ, Liao X, Gao D, Xia JX, Zhang J, Hu B, Yan JA, Wang YJ, Xu M, et al. (2018). The paraventricular thalamus is a critical thalamic area for wakefulness. *Science,* **362**:429-434. DOI: https://doi.org/10.1126/science.aat2512, PMID:30361367

Saper CB. (2016). The house alarm. *Cell Metabolism,* **23**:754-755. DOI: https://doi.org/10.1016/j.cmet.2016.04.021, PMID:27166934

Sun L, Liu R, Guo F, Wen MQ, Ma XL, Li KY, Sun H, Xu CL, Li YY, Wu MY, Zhu ZG, Li XJ, Yu YQ, Chen Z, Li XY, Duan SM. (2020). Parabrachial nucleus circuit governs neuropathic pain-like behavior. *Nature Communications,* **11**. DOI: https://doi.org/10.1038/s41467-020-19767-w, PMID:33239627

Todd AJ. (2010). Neuronal circuitry for pain processing in the dorsal horn. *Nature Review Neuroscience,* **11**:823-836. DOI: https://doi.org/10.1038/nrn2947, PMID:21068766

Tye KM, Prakash R, Kim SY, Fenno LE, Grosenick L, Zarabi H, Thompson KR, Gradinaru V, Ramakrishnan C, Deisseroth K. (2011). Amygdala circuitry mediating reversible and bidirectional control of anxiety. *Nature,* **471**:358-362. DOI: https://doi.org/10.1038/nature09820, PMID:21389985

Vertes RP, Linley SB, Hoover WB. (2015). Limbic circuitry of the midline thalamus. *Neuroscience and Biobehavioral Review,* **54**:89-107. DOI: https://doi.org/10.1016/j.neubiorev.2015.01.014, PMID:25616182

Yamamuro K, Bicks LK, Leventhal MB, Kato D, Im S, Flanigan ME, Garkun Y, Norman KJ, Caro K, Sadahiro M, Kullander K, Akbarian S, Russo SJ, Morishita H. (2020). A prefrontal-paraventricular thalamus circuit requires juvenile social experience to regulate adult sociability in mice. *Nature Neuroscience,* **23**:1240-1252. DOI: https://doi.org/10.1038/s41593-020-0695-6, PMID:32868932

Zhou WJ, Jin Y, Meng Q, Zhu X, Bai TJ, Tian YH, Mao Y, Wang LK, Xie W, Zhong N, Luo M, H., Tao WJ, Wang HT, Li J, Qiu BS, Zhou JN, Li XY, Xu H,

Wang K, Zhang XC, et al. (2019). A neural circuit for comorbid depressive symptoms in chronic pain. *Nature Neuroscience,* **22**:1649-1658. DOI: https://doi.org/10.1038/s41593-019-0468-2,

Zhu Y, Nachtrab G, Keyes PC, Allen WE, Luo L, Chen X. (2018). Dynamic salience processing in paraventricular thalamus gates associative learning. *Science,* **362**:423-429. DOI: https://doi.org/10.1126/science.aat0481, PMID:30361366

Zhu Y, Wienecke CF, Nachtrab G, Chen X. (2016). A thalamic input to the nucleus accumbens mediates opiate dependence. *Nature,* **530**:219-222. DOI: https://doi.org/10.1038/nature16954, PMID:26840481

Zhu Y, Xu L, Wang Y, Zhang Rui, Wang Yuchen, Li Jinbao, D. M. (2020). Posterior thalamic nucleus mediates facial histaminergic itch. *Neuroscience,* **444**:54-63. DOI: https://doi.org/10.1016/j.neuroscience.2020.07.048, PMID:32750381

Zingg B, Chou XL, Zhang ZG, Mesik L, Liang F, Tao HW, Zhang LI. (2017). AAV-Mediated anterograde transsynaptic tagging: mapping corticocollicular input-defined neural pathways for defense behaviors. *Neuron,* **93**:33-47. DOI: https://doi.org/10.1016/j.neuron.2016.11.045, PMID:27989459

Figures and figure legends

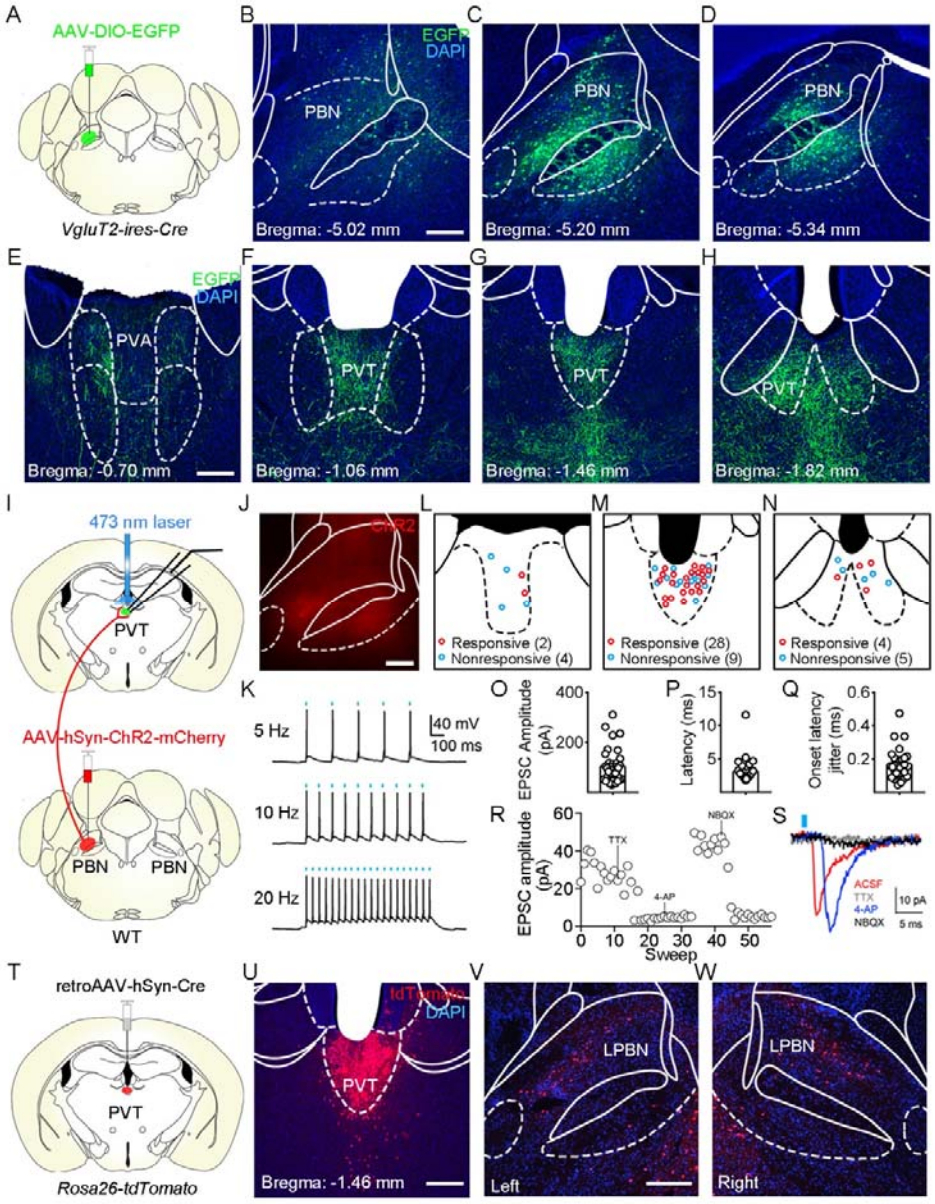

Figure 1. Functional connectivity pattern of the PBN-PVT projection. (A) The illustration for virus injection of AAV2/8-EF1a-DIO-EGFP into the PBN nucleus on *VgluT2-ires-Cre* mice. (B−D) The transduction state of the glutamatergic neurons labeled with EGFP in the PBN. PBN, parabrachial nucleus. Scale bar: 200 μm. (E−H) The distribution pattern of PBN projection fibers in the PVT. PVA, anterior paraventricular thalamus; PVT, paraventricular thalamus. Scale bar: 200 μm. (I) The schematic for virus injection of

AAV2/8-hSyn-ChR2-mCherry into PBN nucleus and the slice recording with 473 nm laser stimulation. (J) The AAV2/8-hSyn-ChR2-mCherry virus expression in the acute PBN slice. Scale bar: 200 μm. (K) 473 nm laser-induced time-locked action potential firing at 5 Hz (top), 10 Hz (middle), and 20 Hz (bottom) in ChR2-expressing neuron in the PBN. Scale bars: 100 ms, 40 mV. (L−N) The locations of the recorded cells in the anterior PVT (L), the middle PVT (M), and the posterior PVT (N). (O−Q) The amplitude of light-evoked EPSCs (O), the average latency of EPSCs (P), and the onset latency jitter of EPSCs (Q) from all 34 responsive neurons in the PVT. (R and S) Example of light-evoked EPSC recorded from a PVT neuron at a holding potential of −70 mV (left panel). The light-evoked EPSC was completely blocked by 1 μM TTX, rescued by 100 μM 4-AP, and blocked by 10 μM NBQX (AMPA/kainate receptor antagonist). Scale bars: 5 ms, 10 pA. (T) Schematic shows retroAAV2/2-hSyn-Cre injection into the PVT nucleus on *Rosa26-tdTomato* mice. (U) The injection site in the PVT nucleus. Scale bar: 200 μm. (V and W) The distribution of the tdTomato positive neurons in the left PBN (V) and the right PBN (W). Scale bar: 200 μm. Data were represented as mean ± SEM.

The following figure supplement is available for figure 1:

Figure supplement 1. Dissection of the brain areas projected to the PVT.

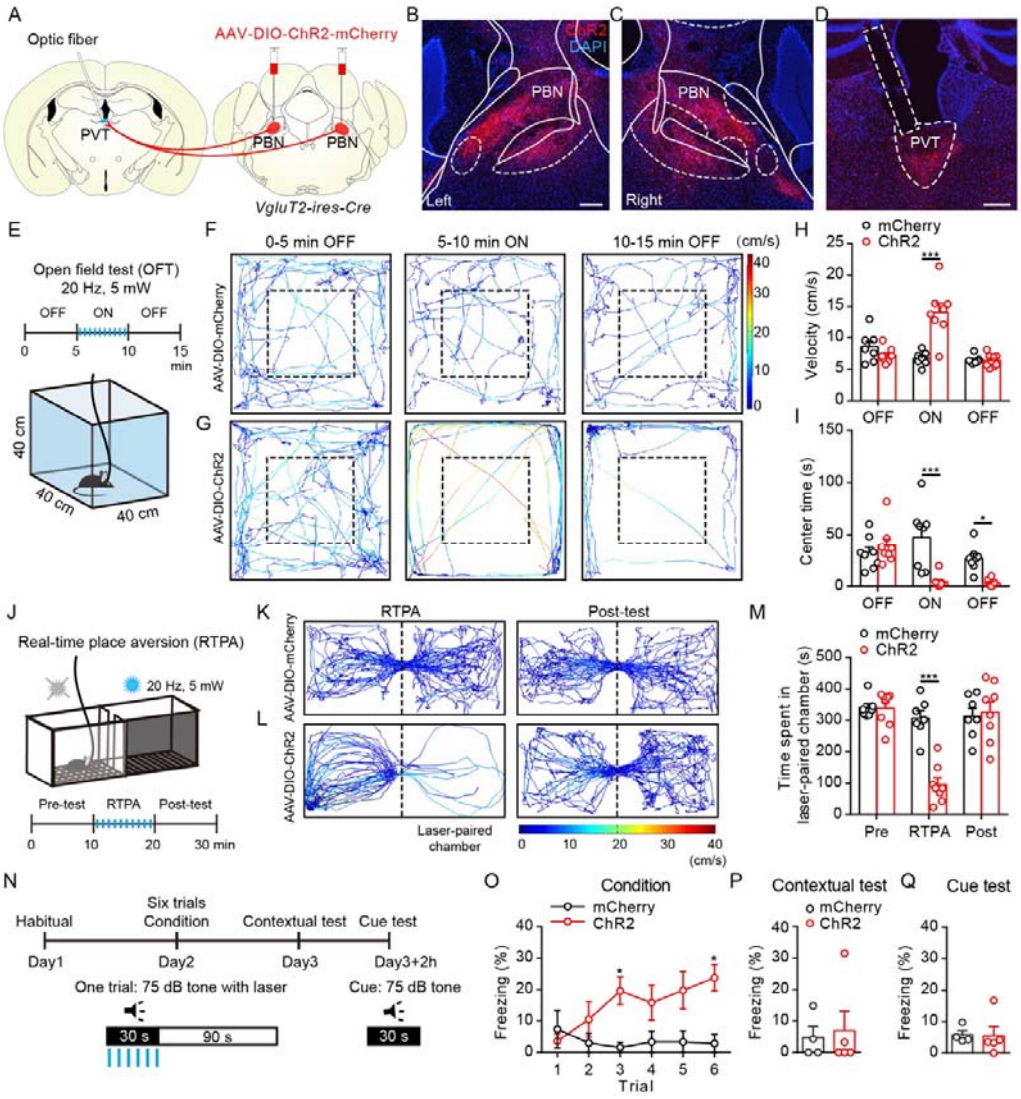

Figure 2. Optogenetics activation of the PBN-PVT projection induced negative emotional states. (A) The illustration shows injection of AAV2/9-EF1a-DIO-ChR2-mCherry virus into the PBN nucleus and the optic fiber tip above the PVT on the *VglutT2-ires-Cre* mice. (B and C) The virus injection sites of the left PBN (B) and the right PBN (C). Scale bar: 200 μm. (D) The projection axons from the PBN and the location of the optic fiber (rectangle) in the PVT. Scale bars: 200 μm. (E) The schematic of the open field test (OFT) with optogenetics activation via a 473 nm laser. (F and G) The example traces of the 15 minutes optogenetics manipulation OFT from an AAV2/9-EF1a-DIO-mCherry virus injected mouse (F) or an

AAV2/9-EF1a-DIO-ChR2-mCherry virus injected mouse (G). (H and I) Quantification of the velocity (H) and the center time (I) in the OFT, *n* = 7−8 mice per group. (J) The illustration of the real-time place aversion test (RTPA) with optogenetics activation via a 473 nm laser. The right side is paired with the laser. (K and L) The example traces of the RTPA and post-test from the mice injected with AAV2/9-EF1a-DIO-mCherry (K) or AAV2/9-EF1a-DIO-ChR2-mCherry (L). (M) Quantification of the time spent in the laser-paired chamber in the pre-test (Pre), RTPA, and post-test (Post), *n* = 7−8 mice per group. (N) Schematic timeline of cue-dependent optogenetic conditioning. (O) Conditioned-freezing responses to sound cue paired with optogenetics activation of projection fibers from the PBN in the PVT during training, *n* = 4−5 mice per group. (P and Q) Optogenetics activation of the projection fibers from the PBN in the PVT did not produce context-dependent fear (P) and cue-dependent fear (Q), *n* = 4−5 mice per group. *p < 0.05, ***p < 0.001, all data were represented as mean ± SEM. Two-way ANOVA followed by Bonferroni test for H, I, M and O. Unpaired student's *t*-test for P and Q.

The following figure supplements are available for figure 2:

Figure supplement 1. The virus expression in the PBN and the optic fiber position in the PVT of mice injected with AAV2/9-EF1a-DIO-ChR2-mCherry or AAV2/9-EF1a-DIO-mCherry.

Figure supplement 2. Effects of optogenetics activation of PBN-PVT projection fibers in the OFT.

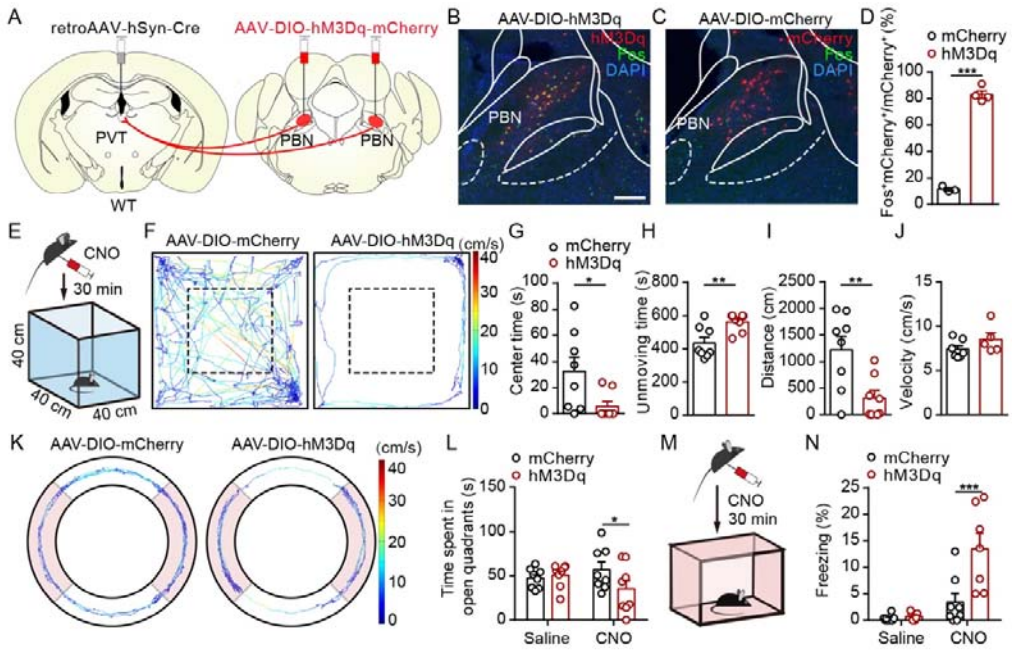

Figure 3. Pharmacogenetics activation of the PVT-projecting PBN neurons generated anxiety-like behaviors and fear-like freezing behaviors. (A) The illustration shows virus injection of retroAAV2/2-hSyn-Cre into the PVT nucleus and bilateral injection of AAV2/9-hSyn-DIO-hM3Dq-mCherry into the PBN nucleus. (B and C) CNO administration evokes Fos expression in AAV2/9-hSyn-DIO-hM3Dq-mCherry injected mice (B) but not in AAV2/9-EF1a-DIO-mCherry injected mice (C). Scale bar: 200 μm. (D) Percentage of co-labeled neurons in the PBN, *n* = 3−4 mice per group. (E) The illustration of the OFT test with pharmacogenetics activation. (F) Example of the OFT traces from the mice infected with AAV2/9-EF1a-DIO-mCherry or AAV2/9-hSyn-DIO-hM3Dq-mCherry. (G-J) Quantification of the time spent in center (G), the unmoving time (H), the total distance (I) and the velocity (J) in the OFT, *n* = 7−8 mice per group. (K) Example elevated zero maze (EZM) traces from the mice infected with AAV2/9-EF1a-DIO-mCherry and AAV2/9-hSyn-DIO-hM3Dq-mCherry. (L) Quantification of the time spent in open quadrants in the EZM test, *n* = 7−8 mice per group. (M) The illustration of pharmacogenetics activation-induced fear-like freezing behavior. (N) Pharmacogenetics activation of PVT-projecting PBN neurons induced fear-like

freezing behaviors, *n* = 7−8 mice per group. *p < 0.05, **p < 0.01, ***p < 0.001, all data were represented as mean ± SEM. Unpaired Student's *t*-test for D, G, H, I and J. Two-way ANOVA followed by Bonferroni test for L and N.

The following figure supplements are available for figure 3:

Figure supplement 1. The PVT-projecting PBN neurons did not send efferents to CeA.

Figure supplement 2. The virus expression in the PBN of mice injected with AAV2/9-hSyn-DIO-hM3Dq-mCherry or AAV2/9-EF1a-DIO-mCherry in the pharmacogenetics manipulation.

Figure supplement 3. Pharmacogenetics activation of PVT-projecting PBN neurons did not affect depressive-like behaviors, basal nociceptive thresholds, formalin-induced licking behavior or the motor ability.

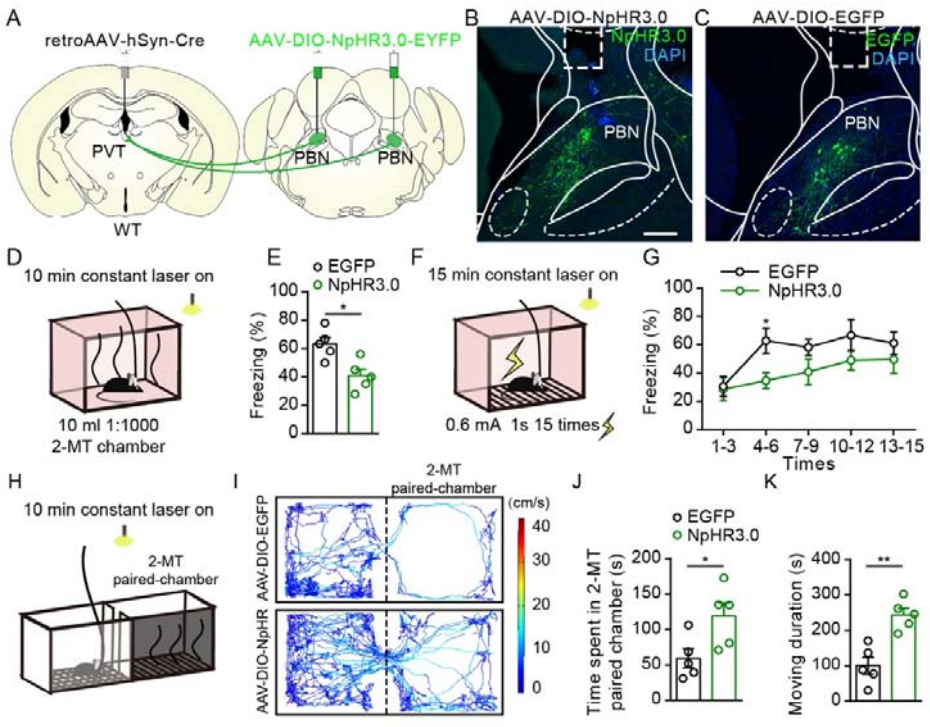

Figure 4. Optogenetics inhibition of the PBN-PVT projection rescued the fear-like freezing behavior and aversion-like behaviors. (A) The illustration shows virus injection of retroAAV2/2-hSyn-Cre into the PVT and bilateral injection of AAV2/9-EF1a-DIO-NpHR3.0-EYFP into the PBN, and bilateral

placement of fiber optic tip above the PBN on WT mice. (B and C) Examples of AAV2/9-EF1a-DIO-NpHR3.0-EYFP (B) and AAV2/8-EF1a-DIO-EGFP (C) expression in the PBN, the rectangle represented the position of the optic fiber. Scale bar: 200 μm. (D) Schematic of 2-MT induced fear-like behavior with optogenetics inhibition via a 589 nm laser. (E) Quantification of the freezing behavior, *n* = 5 mice per group. (F) Illustration of footshock-induced freezing behavior with optogenetics inhibition via a 589 nm laser. (G) Quantification of the freezing behavior, *n* = 5 mice per group. (H) Schematic of 2-MT induced aversion test with optogenetics inhibition via a 589 nm laser. (I) Representative traces of the mice infected with AAV2/8-EF1a-DIO-EGFP or AAV2/9-EF1a-DIO-NpHR3.0-EYFP in the chamber. (J and K) Quantification of the time spent in the 2-MT paired chamber (J) and the moving duration (K), *n* = 5 mice per group. *p < 0.05, **p < 0.01, all data were represented as mean ± SEM. Unpaired Student's *t*-test for E, J and K. Two-way ANOVA followed by Bonferroni test for G.

The following figure supplement is available for figure 4:

Figure supplement 1. Optogenetics inhibition of PBN-PVT projection did not affect basal emotional state and locomotion.

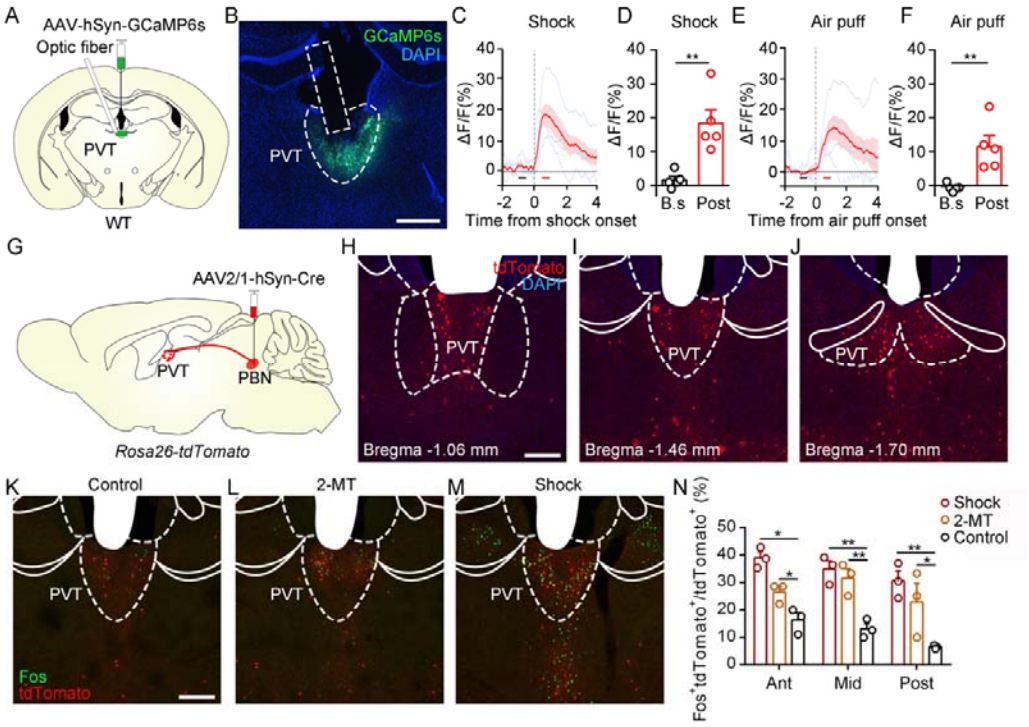

Figure 5. Activation of PVT_{PBN} by diverse aversive stimuli. (A) Schematic shows injection of AAV2/8-hSyn-GCaMP6s into the PVT and placement of the optic fiber above the PVT. (B) Representative of GCaMP6s expression and the position of optic fiber in the PVT. Scale bar: 400 μm. (C and D) The calcium signal of the PVT neurons (C) and the quantification of the average Ca^{2+} signal before and after footshock (D). The black bar represented the baseline period (B.s, -1 to -0.5 s), and the red bar represented the post-stimulus period (Post, 0.5 to 1 s), *n* = 5 mice. (E and F) The calcium signal of the PVT neurons (E) and the quantification of average Ca^{2+} signal before and after air puff (F), The black bar represented the baseline period (B.s, -1 to -0.5 s), and the red bar represented the post-stimulus period (Post, 0.5 to 1 s), *n* = 5 mice. (G) The illustration shows the injection of AAV2/1-hSyn-Cre into the PBN of *Rosa26-tdTomato* mice. (H−J) The distribution of the neurons received projection from the PBN in the PVT at brain level of bregma -1.06 mm(H), bregma -1.46 mm (I) and bregma -1.70 mm(J). Scale bar: 200 μm. (K−M) The Fos induced by habituation control (K), 2-MT (L), or shock (M) co-labeled with the tdTomato positive neurons in the PVT. Scale bar: 200 μm. (N)

Quantification of the co-labeled neurons, *n* = 3 mice per group. *p < 0.05, **p < 0.01, all data were represented as mean ± SEM. Paired Student's *t*-test for D and F. Unpaired Student's *t*-test for N.

The following figure supplement is available for figure 5:

Figure supplement 1. The downstream areas of PBN neurons.

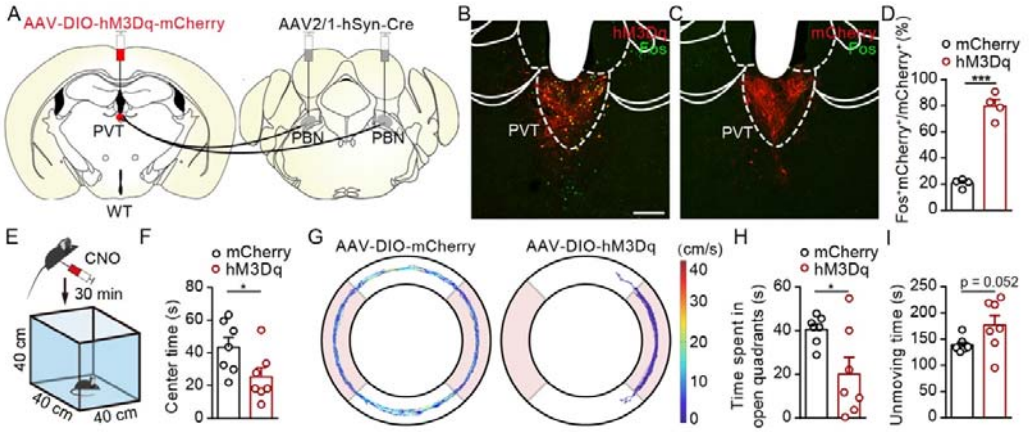

Figure 6. Activation of PVT_{PBN} neurons induced anxiety-like behaviors. (A) Illustration shows injection of AAV2/1-hSyn-Cre into the PBN and AAV2/9-hSyn-DIO-hM3Dq-mCherry into the PVT. (B and C) CNO administration evokes Fos expression in AAV2/9-hSyn-DIO-hM3Dq-mCherry injected mice (B) but not in AAV2/9-EF1a-DIO-mCherry injected mice (C). Scale bar: 200 μm. (D) Percentage of co-labeled neurons in the PVT, *n* = 4 mice per group. (E) The illustration of the OFT test with pharmacogenetics activation. (F) Quantification of center time in the OFT, *n* = 7 mice per group. (G) Example elevated zero maze (EZM) traces from the mice injected with AAV2/9-EF1a-DIO-mCherry or AAV2/9-hSyn-DIO-hM3Dq-mCherry. (H and I) Quantification of the time spent in open quadrants (H) and the unmoving time in EZM test (I), *n* = 7 mice per group. *p < 0.05, ***p < 0.001, all data were presented as mean ± SEM. Unpaired Student's *t*-test for D, F, H and I.

The following figure supplement is available for figure 6:

Figure supplement 1. Distribution pattern of projection fibers of PVT_{PBN} neurons.

Supplemental information

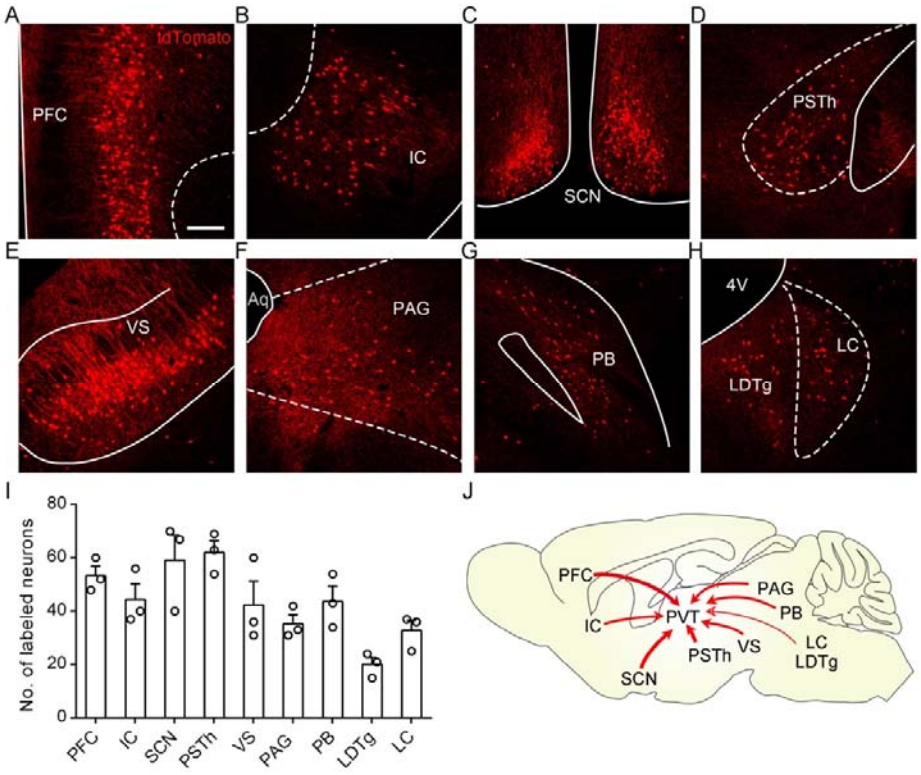

Figure1−figure supplement 1. Dissection of the brain areas projected to the PVT. (A−H) Representative images of retrogradely tdTomato labeled neurons in PFC (A), IC (B), SCN (C), PTSh (D), VS (E), PAG (F), PB (G), LC (H), and LDTg (H). PFC, prefrontal cortex; IC, insular cortex; SCN, suprachiasmatic nucleus; PTSh, parasubthalamic nucleus; VS, ventra subiculum; PAG, periaqueductal gray; PB, parabrachial nucleus; LC, locus coeruleus; LDTg, laterodorsal tegmental nucleus. Scale bar: 200 μm. (I) Quantification of the tdTomato labeled neurons in these brain areas, *n* = 3 mice. (J) Schematic of the brain areas innervated the PVT. Data were represented as mean ± SEM.

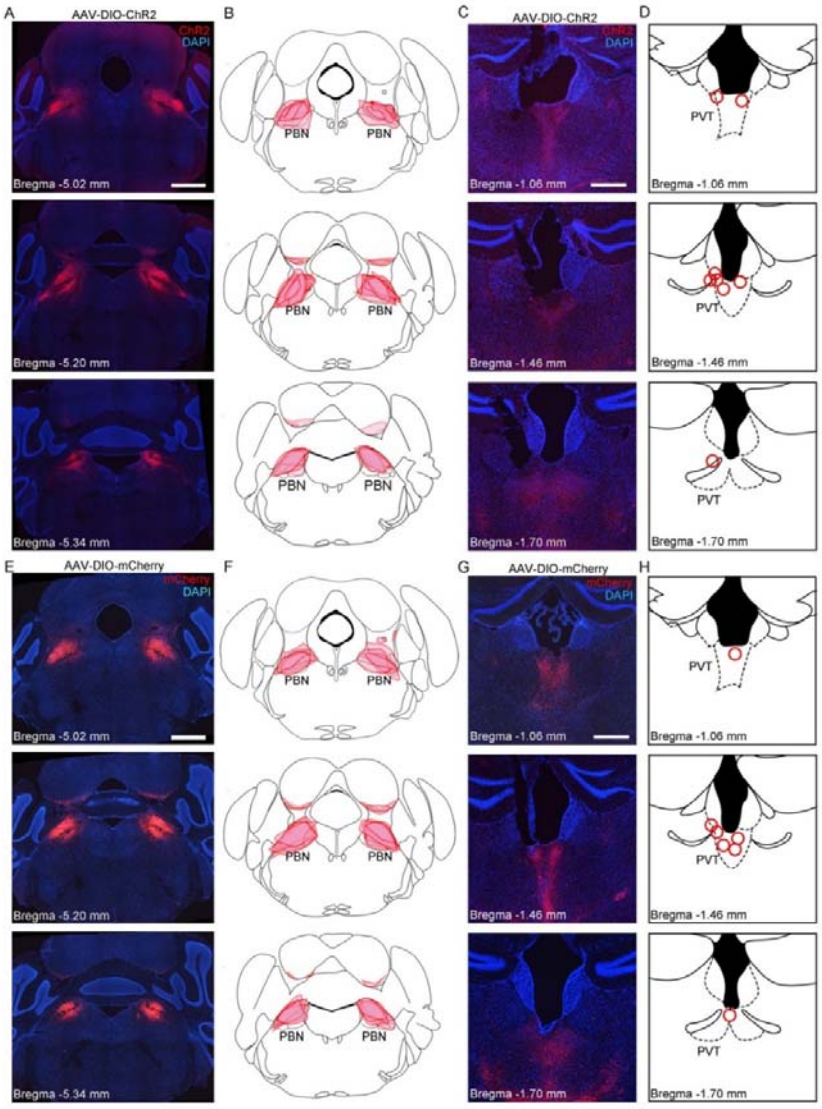

Figure 2−figure supplement 1. The virus expression in the PBN and the optic fiber position in the PVT of mice injected with AAV2/9-EF1a-DIO-ChR2-mCherry or AAV2/9-EF1a-DIO-mCherry.

(A) Representative images of ChR2 expression from bregma −5.02 mm to bregma −5.34 mm from one mouse. Scale bar: 1 mm. (B) Superimposed depiction of virus infection areas from 8 mice. (C) Representative images of optic fiber position in bregma −1.06 mm, −1.46 mm, and −1.70 mm from 3 AAV2/9-EF1a-DIO-ChR2-mCherry injected mice. Scale bar: 1 mm. (D) Position of the optic fiber tip (red circle) from eight AAV2/9-EF1a-DIO-ChR2-mCherry infected mice. (E) Representative images

of mCherry expression from bregma −5.02 mm to bregma −5.34 mm from one mouse. Scale bar: 1 mm. (F) Superimposed depiction of virus infection areas from 7 mice. (G) Representative images of optic fiber position in bregma −1.06 mm, −1.46 mm, and −1.70 mm from 3 mice injected with AAV2/9-EF1a-DIO-mCherry. Scale bar: 1 mm. (H) Position of the optic fiber tip from 7 mice injected with AAV2/9-EF1a-DIO-mCherry.

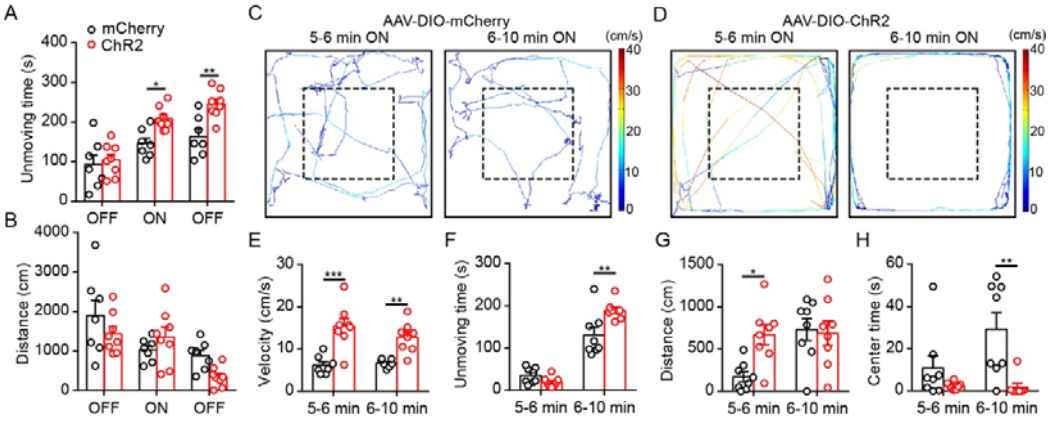

Figure 2−figure supplement 2. Effects of optogenetics activation of PBN-PVT projection fibers in the OFT. (A and B) Quantification of the unmoving time (A) and the distance (B) in the OFT (*n* = 7−8 mice per group). (C and D) Representative traces of an AAV2/9-EF1a-DIO-mCherry infected mouse (C) and an AAV2/9-EF1a-DIO-ChR2 infected mouse (D) during the 5−6 minute and the 6−10 minutes laser on period in the OFT test. (E−H) Quantification of the velocity (E), the unmoving time (F), the distance (G), and the center time (H) during the 5−6 minute and the 6−10 minutes laser on period in the OFT test (*n* = 7−8 mice per group). *p < 0.05, **p < 0.01, ***p < 0.001, all data were represented as mean ± SEM. Two-way ANOVA followed by Bonferroni test for A, B, E, F, G and H.

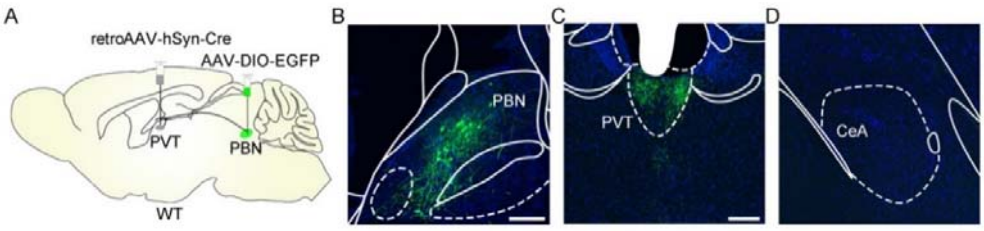

Figure 3−figure supplement 1. The PVT-projecting PBN neurons did not send efferents to CeA. (A) Illustration shows the injection of retroAAV2/2-hSyn-Cre into the PVT and AAV2/8-EF1a-DIO-EGFP into the PBN to label the PVT-projecting PBN neurons. (B) Examples of AAV2/8-EF1a-DIO-EGFP expression in the PBN. Scale bar: 200 μm. (C and D) The efferents from the PVT-projecting PBN neurons could be found in the PVT (C) but not in the CeA (D). Scale bar: 200 μm.

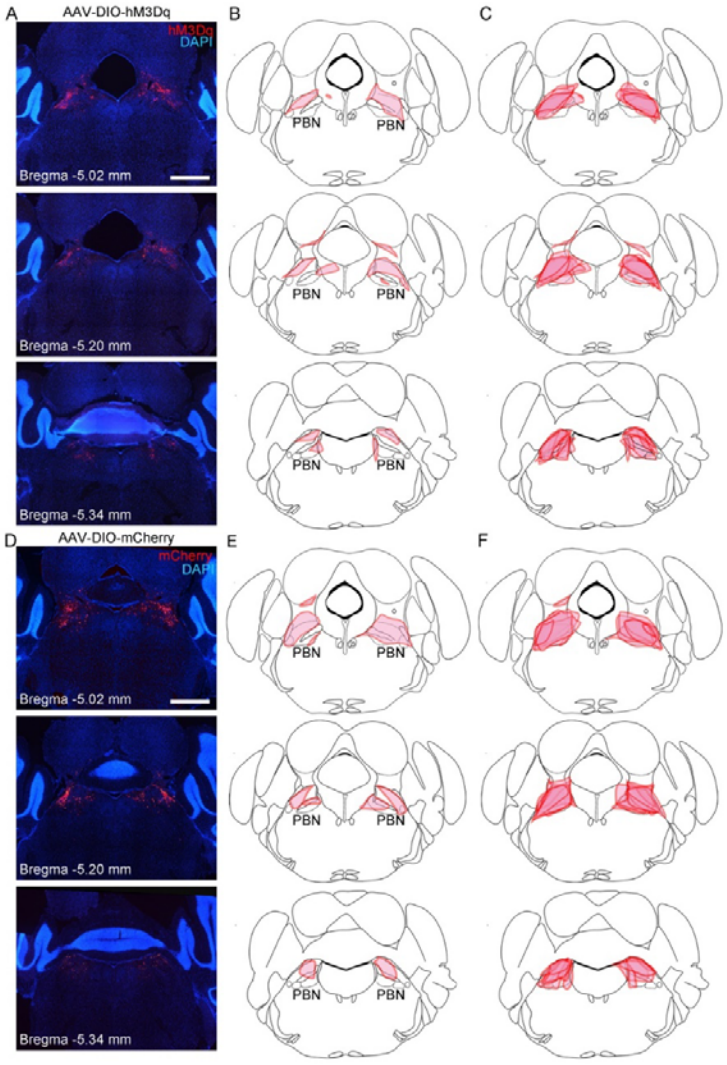

Figure 3−figure supplement 2. The virus expression in the PBN of mice injected with AAV2/9-hSyn-DIO-hM3Dq-mCherry or AAV2/9-EF1a-DIO-mCherry in the pharmacogenetics manipulation. (A) Representative histological images of hM3Dq expression in an AAV2/9-hSyn-DIO-hM3Dq-mCherry injected mouse at brain level from bregma −5.02 mm to bregma −5.34 mm. Scale bar: 1 mm. (B) Depiction of virus infection area according to the histological images in (A). (C) Superimposed depiction of virus transduction from 8 mice. (D) Representative histological images of mCherry expression in AAV2/9-EF1a-DIO-mCherry injected mice at brain level from bregma −5.02 mm to bregma −5.34 mm. Scale bar: 1 mm. (E) Depiction of virus infection area according to the histological images in (D). (F)

Superimposed depiction of virus transduction from 8 mice.

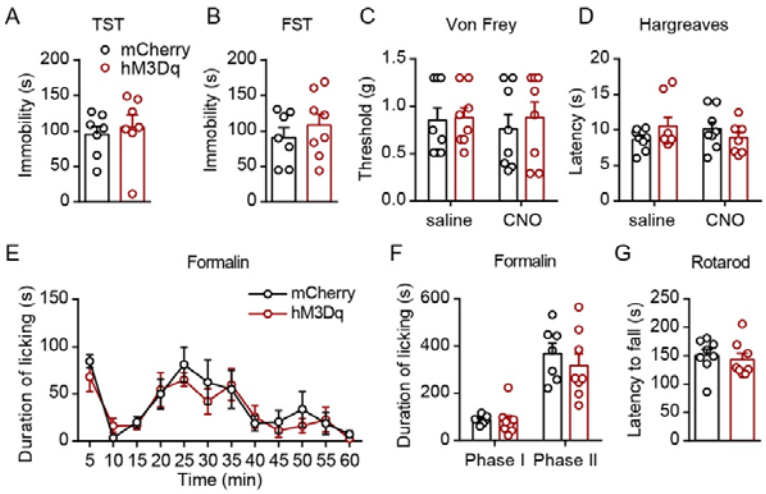

Figure 3−figure supplement 3. Pharmacogenetics activation of PVT-projecting PBN neurons did not affect depressive-like behaviors, basal nociceptive thresholds, formalin-induced licking behavior or the motor ability. (A and B) Immobility time in the tail suspension test (TST, A) and forced swimming test (FST, B), *n* = 7−8 mice per group. (C and D) Effects of pharmacogenetics activation of PVT-projecting PBN neurons on the nociceptive response tested by Von Frey (C) and Hargreaves (D), *n* = 7−8 mice per group. (E and F) Duration of licking behaviors in the formalin-induced inflammatory pain test, *n* = 7−8 mice per group. Phase I: 0−10 minutes, Phase II: 10−60 minutes. (G) The locomotor in the rotarod test, *n* = 7−8 mice per group. Data were represented as mean ± SEM. Unpaired student's *t*-test for A, B and G. Two-way ANOVA followed by Bonferroni test for C, D, E and F.

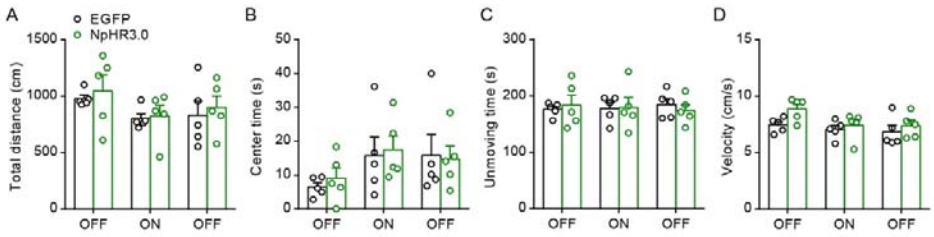

Figure 4−figure supplement 1. Optogenetics inhibition of PBN-PVT projection did not affect basal emotional state and locomotion. (A−D) Optogenetics inhibition of PBN-PVT projection didn't affect the distance (A), the center time (B), the unmoving time (C), and the velocity (D) in the OFT test, *n* = 5 mice per group. Data were presented as mean ± SEM. Two-way ANOVA followed by Bonferroni test for A, B, C and D.

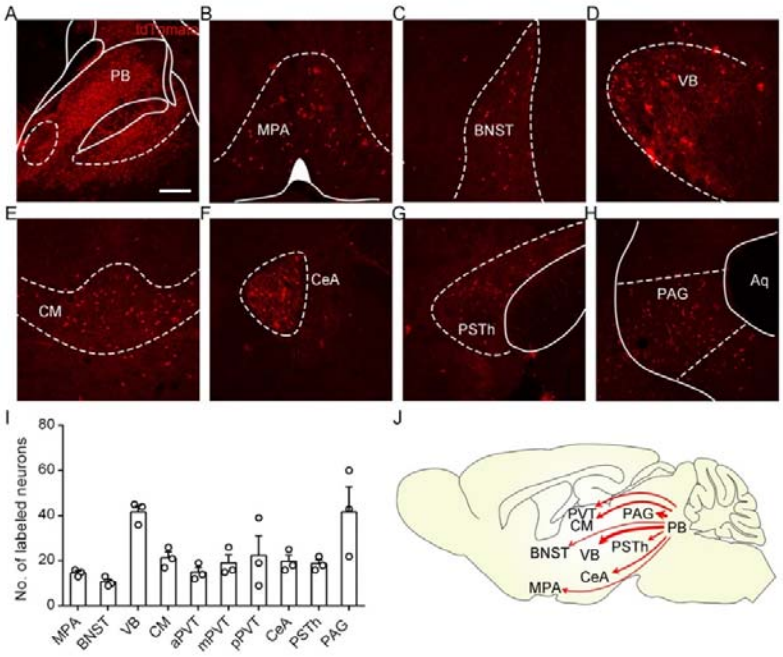

Figure 5−figure supplement 1. The downstream areas of PBN neurons. (A) The virus expression in the PBN nucleus. Scale bar: 200 μm. (B−H) The distribution of the labeled tdTomato positive neurons in MPA (B), BNST (C), VB (D), CM (E), CeA (F), PSTh (G), and PAG (H). MPA, medial preoptic area; BNST, bed nucleus of the stria terminalis; VB, ventrobasal complex of the thalamus; CM, central medial thalamus nucleus; CeA, central nucleus of the amygdala; PSTh, parasubthalamic nucleus; PAG, periaqueductal gray. (I) Quantification of the labeled neurons in these brain areas, *n* = 3 mice. (J) Schematic of the brain regions innervated by the PBN. Data were represented as mean ± SEM.

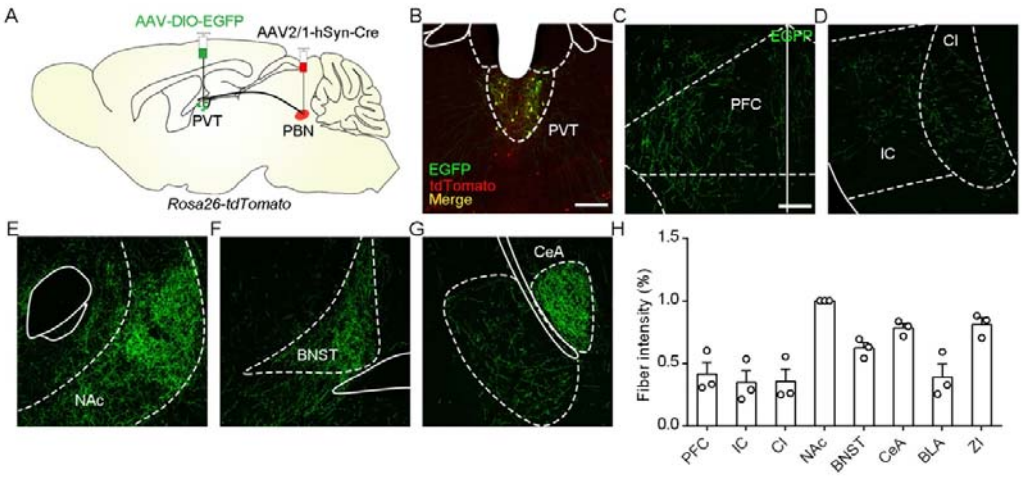

Figure 6−figure supplement 1. Distribution pattern of projection fibers of PVT_{PBN} neurons. (A) Illustration shows injection of AAV2/1-hSyn-Cre into the PBN and AAV2/8-EF1a-DIO-EGFP into the PVT. (B) The representative image of EGFP and tdTomato-transduced neurons in the PVT. Scale bar: 200 μm. (C−G) Distribution patterns of EGFP fibers in the PFC (C), IC (D), CI (D), NAc (E), BNST (F), and CeA (G). PFC, prefrontal cortex; IC, insular cortex; CI, claustrum; NAc, nucleus accumbens core; BNST, bed nucleus of the stria terminalis; CeA, central nucleus of the amygdala. Scale bar: 200 μm. (H) Quantification of the fiber intensity in these brain regions, *n* = 3 mice. Data were represented as mean ± SEM.